NLTH and NLPO analyses of Building B
Module 3 – Harmonisatie berekeningsmethode

Longo, M.; Singla, A.; Messali, F.

Publication date
2020

Document Version
Final published version

Citation (APA)
Longo, M., Singla, A., & Messali, F. (2020). *NLTH and NLPO analyses of Building B: Module 3 – Harmonisatie berekeningsmethode*. Delft University of Technology.

Project number	CM1B13
File reference	CM1B13-R01
Date	19 October 2020
Corresponding author	Francesco Messali (f.messali@tudelft.nl)

Module 3 – Harmonisatie berekeningsmethode

NLTH AND NLPO ANALYSES OF BUILDING B

Authors: Michele Longo, Anmol Singla, Francesco Messali

***Cite as**: Longo, M., , Singla, A., Messali, F. NLTH and NLPO analyses of Building B - Module 3 – Harmonisatie berekeningsmethode. Report no. CM1B13-R01, Version 08, 19 October 2020. Delft University of Technology*

This document is made available via the website 'Structural Response to Earthquakes' and the TU Delft repository. While citing, please verify if there are recent updates of this research in the form of scientific papers.

This research work was funded by y Stichting Koninklijk Nederlands Normalisatie Instituut (NEN) under project number 8505400024-001.

Table of Contents

1 INTRODUCTION

This report summarizes the results for the numerical analyses of Building B in support to the development of NPR 9998 Module 3.

The following analysis types are carried out:

1. Non-linear pushover (NLPO) "full FEM"[1] analyses for both uniform and modal distributed loads;
2. Non-linear time history (NLTH) "full FEM" analyses;
3. Simplified Lateral Mechanism Analyses (SLaMA).

The following assumptions are considered:

- Backbone curves of piers and spandrels defined according to NPR 9998;
- Global and local acceptance criteria based on Annex G of NPR 9998;
- Indirect compliance assessment method as defined in Annex F of NPR 9998;
- Fixed based boundary conditions;
  Spectrum according to the Webtool.

The NLTH analyses consider both the original site-specific input ground motion, and a scaled ground motion.

For the sake of simplicity, where the following text refers to an article, a section or an Annex "of NPR", this is in fact referring to NPR 9998 [2].

1.1 Analysis Method

Both the NLPO and NLTH analyses were carried out using the non-linear finite element analysis program DIANA FEA, version 10.3. The building was modelled in 3D using shell and beam elements. For the masonry material, a non-linear orthotropic total strain based model was used, which is able to reproduce cracking, crushing and shear behaviour of masonry [1]. The materials of the concrete floors, including the rebars, were also modelled as non-linear. Elastic properties of the roof structure properties were taken from calibrated parameters based on similar laboratory experiments. Further details on the DIANA modelling approach are provided in Section 2.1.

1.2 NPR 9998 Acceptance Criteria

Both global and local acceptance criteria are considered. Global criteria are applied to the building as a whole and to the associated capacity curve. Local criteria are applied to specific elements, such as piers and spandrels.

1.2.1 Global acceptance criteria

The exceedance of the NC limit state is defined in Section G.6.1 of NPR. This occurs when:

- The total lateral force resistance has reduced by 50% relative to the maximum value.
- A number of load-bearing elements has exceeded its displacement capacity leading to partial or full building collapse.
- The drift limits defined according to table G.2 of NPR are exceeded.

Other global criteria referred to the diaphragms are given in article G.9.5.2(2) of NPR.

1.2.2 Local acceptance criteria

The local acceptance criteria for piers are considered as recommended in sections G.9.2.2 and G.9.2.3 of NPR. As regards the masonry spandrels, these are assumed not to be essential to the stability of the load-bearing system. Therefore, a maximum drift of 2% is assigned to rectangular spandrels. This is in accordance with section G.9.3.1(8) of NPR, and applies to both non-load bearing and load-bearing spandrels.

[1] As defined in Annex G of NPR 9998.

1.3 Boundary Conditions

Building B is evaluated without considering the soil-structure interaction (SSI) effects, and a fixed based analysis is performed.

2 MODEL DESCRIPTION AND INPUT DATA

2.1 Building Overview and Modelling Approach

Building B comprises three terraced units, built in 1973. The building is made of unreinforced masonry (URM) cavity walls. Additionally, three appendices and an extra one-storey building are part of the entire structure. A picture and a plane section of the building is shown in Figure 1. Summary information about the building information is provided in Table 1.

Figure 1. Building B terraced house.

Table 1. Building B – Summary of the model building information.

Building year	1973
Number of storeys	2 plus attic
Height	8.2 m
Walls	Cavity wall system with wall ties: - Outer leaf: Clay brick - Inner leaf: CaSi brick Internal walls: - Load bearing: CaSi brick - Non-load bearing: CaSi brick
Floors	Ground floor: Kwaaitaal floor 1st floor: in-situ reinforced concrete slab 2nd floor (attic): in-situ reinforced concrete slab
Roof	Timber purlins and trusses with concrete roof tiles
Roof-to-wall connection	On transversal walls: pocket connection with blind anchors On longitudinal walls: wall plate with friction connection onto masonry wall
Floor-to-wall connection	Fixed connection on both longitudinal and transversal walls – 2-way spanning slabs
Floor-to-roof connection	Roof truss is connected to the attic slab via steel anchors
Total mass	126 t/unit
Footprint area	58 m^2/unit
Material properties	Properties adopted for the unreinforced masonry walls assuming clay brickwork (post-1945) for the outer leaf and CaSi brickwork (1960-present) for the inner leaf properties – see Appendix A1

The terraced house representing the Building B is numerically modelled in 3D by the software Diana 10.3. Since the three units have same dimensions and the inner walls are not interconnected, as well as the concrete floors, only one building unit (left one, highlighted in Figure 1) is modelled. A representation of the model is shown in Figure 2.

The cavity wall system is implemented by explicitly modelling the inner leaf and considering the outer leaf as dynamic mass acting in the direction perpendicular to the wall. The assumption in this case is that the wall ties are not able to transfer any force in the shear direction. The chimney is also included in the model as dynamic mass. The mass density assigned to the different external walls is depicted in Figure 3. All the internal walls are explicitly modelled. The load bearing internal transversal walls, one located at the ground floor and one at the first floor, are fully connected to both bottom and top floor and to the longitudinal external façades. The other internal walls are not bearing any load, thus their top edge is disconnected from the top floor so

that no force will be transfer at that location. In practice, the lateral connection with the transversal external façades is done by a vertical mortar joint. Such connection is modelled with a strip of weak elements that simulates a vertical mortar joints. An overview of the internal walls is shown in Figure 4. Both internal and external walls are modelled using the Engineering Masonry Model [1]. The weak elements representing the joint between internal and external walls are also modelled with the Engineering Masonry Model, but rotating the local axes and with both elastic and nonlinear properties reduced by 30%.
Ground Kwaaitaal floor and first/second floor slabs are modelled as non-linear elements, considering the Total Rotating Strain Crack Model for concrete. The steel reinforcement is modelled as discrete or continues reinforcement using the Von Mises Plasticity model (Figure 5).
In order to include on the external façades the separation between masonry piers at different storey, rigid floor strips with the height equal to the concrete floor thickness are modelled. A linear elastic isotropic material is assigned to such elements (Figure 6). The lintels are also modelled as linear elastic material.
The roof purlins, struts, ties and ridge beam are modelled with beam elements using a linear elastic isotropic material (Figure 7). The connection between the gable and the purlins-ridge beams is modelled with point interface elements to simulate the possible sliding behaviour of the pocket connections. A Coulomb-Friction material model is assigned to the interface elements. The timber boards, representing the roof diaphragm, are modelled as shell elements using linear elastic orthotropic material. On the edges of the roof planks, dummy beams are added to provide numerical stability to the model (Figure 8).

Quadratic 8-noded curved shell elements (CQ40S and CT30S) are used to model the walls, floors and lintels of the 3D building. The timber beams in the roof are modelled with Class-III beam element (CL18B). The model is assumed to be fixed base (no soil-structure interaction is considered), so that it is fully restrained at the bottom from translations and rotations. The elements are meshed with an average size of 200x200 mm (Figure 2).

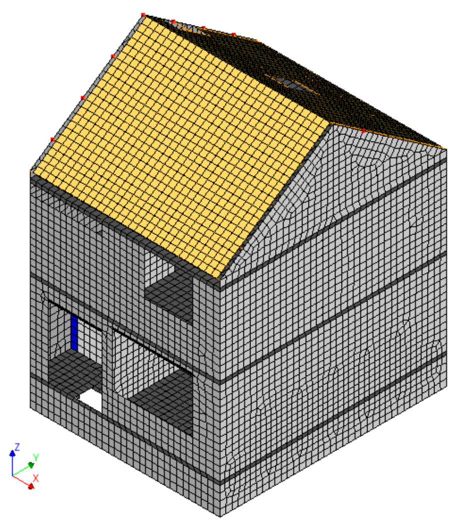

Figure 2. Diana Model of Building B unit.

Non Linear Pushover (NLPO) and Non Linear Time History (NLTH) analyses are conducted. For the NLPO analyses, the model is initially subjected to the gravity loads applied in ten equal steps. Then, either uniform distributed lateral loads, applied via a uniform lateral acceleration, or modal distributed lateral loads, based on the main eigen-mode of the structure (and the corresponding participating mass) obtained via eigen-value analyses, are applied so that an average displacement rate of 0.1 mm/step is recorded at floor level. It should be noted that the uniform lateral acceleration does not account for the extra dynamic mass. The Secant BFGS (Quasi-Newton) method is adopted as iterative method in combination with the Arc-Length control. Both displacement and force norms must be satisfied during the iterative procedure within a tolerance of 1%. For the NLTH analyses, the model is first subjected to gravity loads, again applied in ten equal steps. Then, the different acceleration motions are applied in the longitudinal, transversal and vertical direction at the base nodes, using a time step of 2.5 milliseconds. A Rayleigh damping of 2% is accounted in the calculation. The Secant BFGS (Quasi-Newton) method is employed as iterative method. Energy norm must be satisfied during the iterative procedure with a tolerance of 0.01%. For both analyses, the Parallel Direct Sparse method is employed to solve the system of equations. The second order effects are considered via the Total Lagrange geometrical nonlinearity.

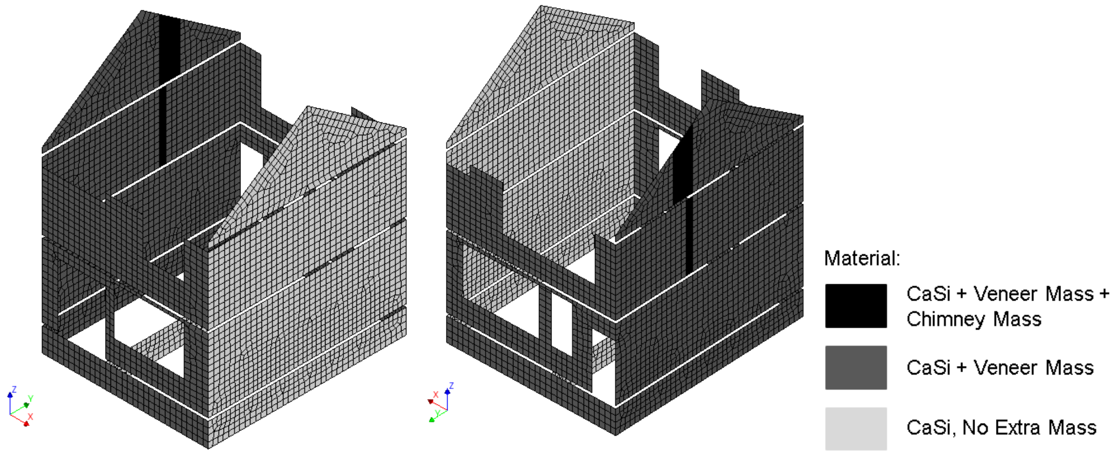

Figure 3. External walls material according to considered mass.

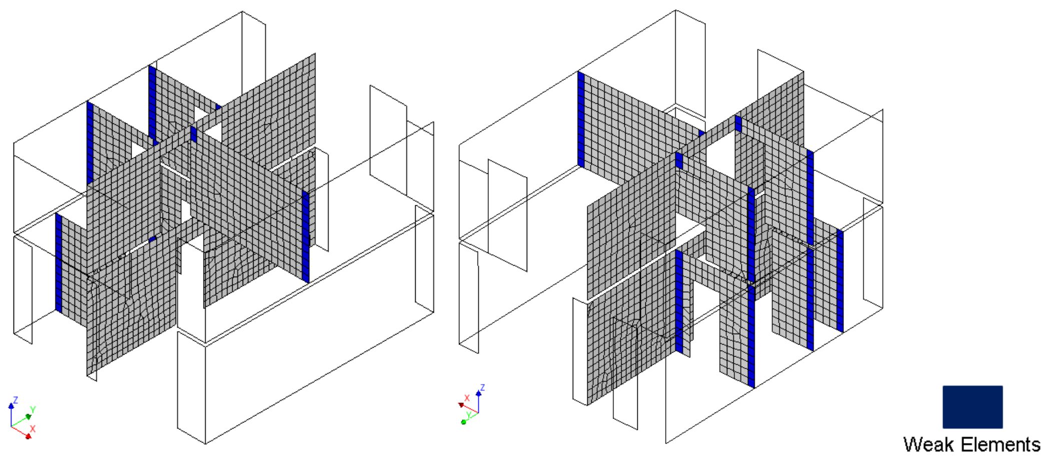

Figure 4. Internal walls. Weak element connection is highlighted in blue.

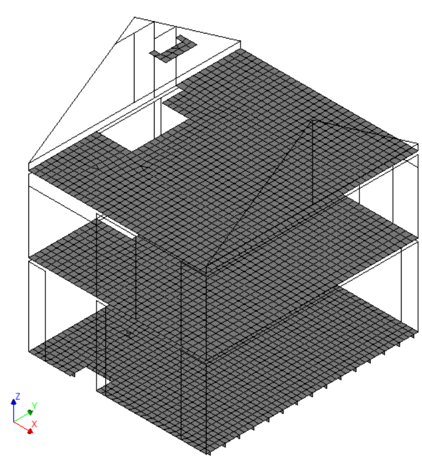

Figure 5. Concrete floors

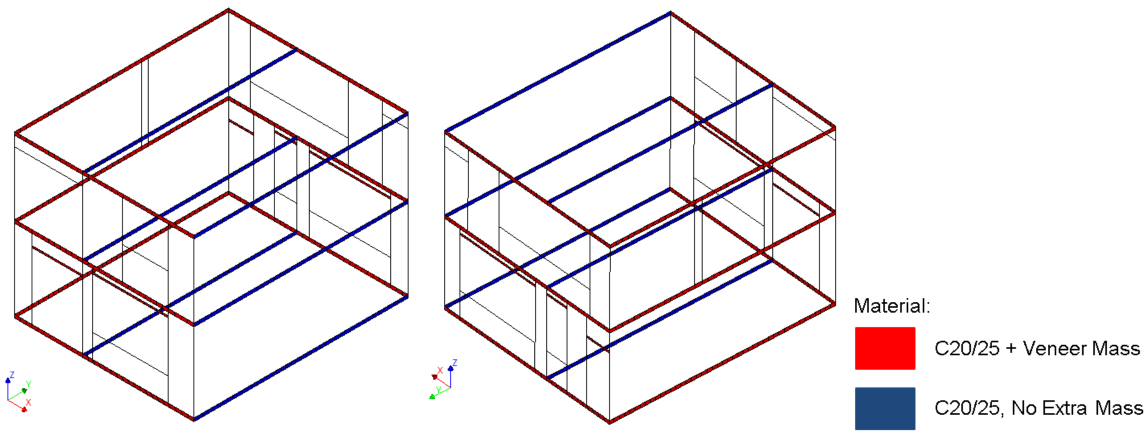

Figure 6. Concrete strips as separation of external masonry at different storey.

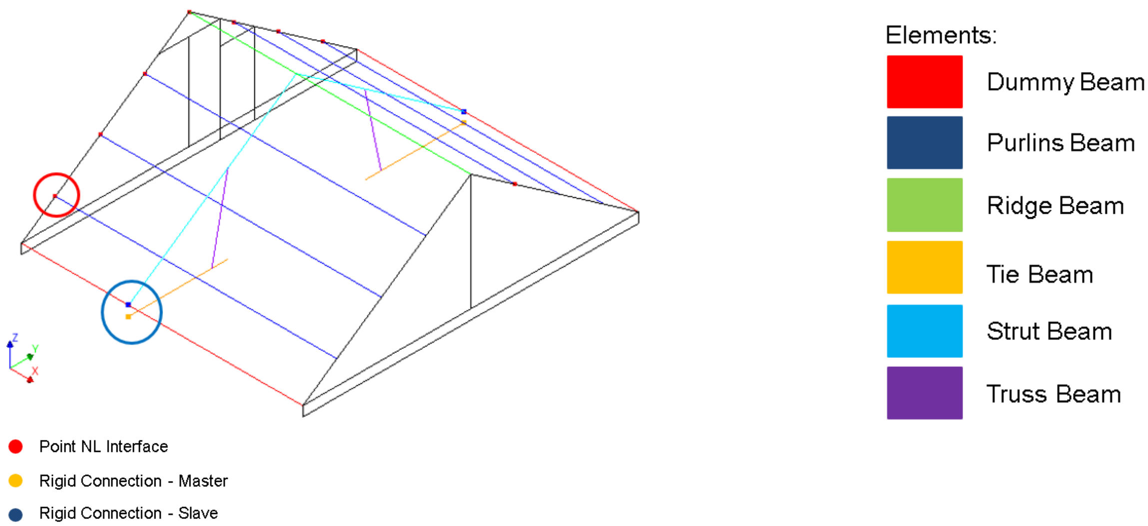

Figure 7. Roof beam structure.

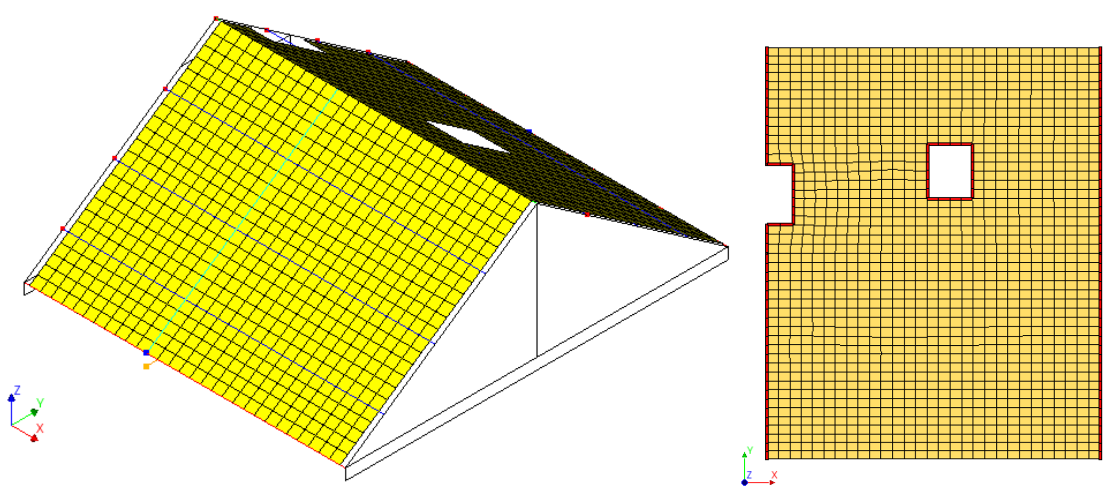

Figure 8. Roof boards and dummy beams.

2.2 Input Ground Motion and Spectrum

The surface level ground motions for the analyses are provided by the NEN web tool NPR 9998 [3]. For each ground motion, three components are provided (two horizontal and one vertical). The horizontal components x and y from the Web tool are aligned with the respective local x and y axes defined for the numerical models. In the case of "fixed base" boundary conditions, the surface level ground motions are applied directly to the base of the building and soil and foundation flexibility effects are not taken into account.
The information on the seismic inputs for the Building B model are summarised in Table 2.
The location of the Building B with respect to the ground motion clusters defined in the NEN web tool is shown in Figure 9. The elastic spectrum obtained from the web tool is shown in Figure 10.

Table 2. Building B: definition of seismic input.

Ground Motion Model	GMMv5 2018-10-01
Return period	2475 years
Time period	T1
Number of ground motions	11 (out of 11)
Ground motion cluster [3]	C
$a_g S$ (unscaled PGA) [3]	0.148g
Importance factor γ_I [1] §2.2.3, Table 2.4	1
Scaling factor for number of GMs (11/11) with indirect check γ_n [1] §F.6.3	1
Scaling factor for number of GMs (11/11) with explicit check γ_n [1] §F.6.2	1.25

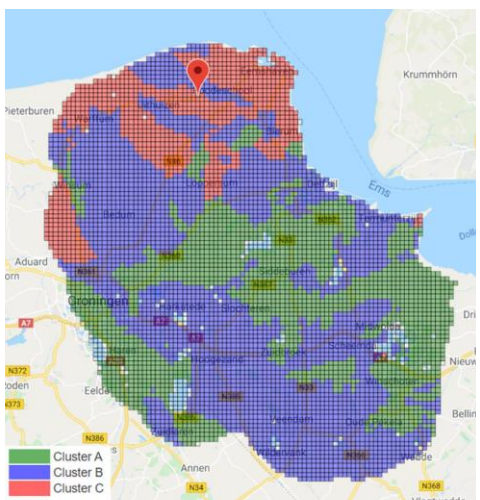

Figure 9. Building B: location of the building from Web tool NPR 2018 with ground motion clustering.

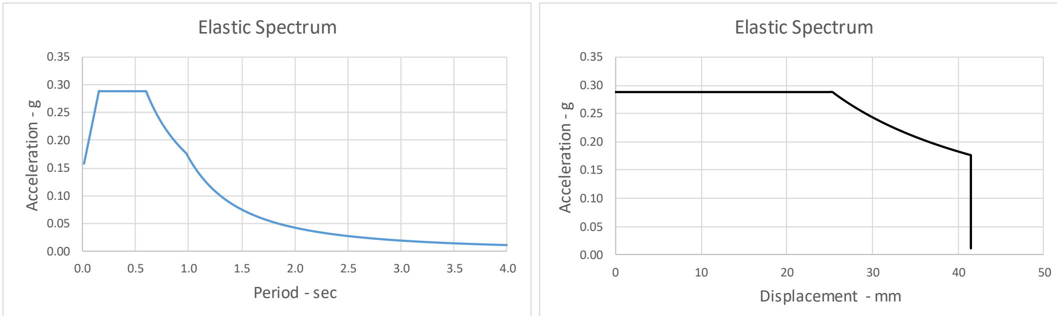

Figure 10. Building B: Elastic spectrum from web-tool.

2.3 Material Properties

The material properties of masonry are taken from Table F.2 of NPR. The masonry quality is considered as excellent [4]. Specific properties related to the Diana FEA material models are listed down below.

2.3.1 Masonry

Masonry is modelled using the Engineering Masonry Model [1]. The model consider the local axis y as the direction perpendicular to the bed joint and Poisson`s ratio equal to zero. The weak material assigned at the interface between internal non-loadbearing and external walls has rotated local axes and lower values of elastic and strength properties. For the NLTH calculations the elastic properties are halved in order to properly capture the cyclic strength degradation, not explicitly described by the EMM. Besides, the same assumption has been already employed in other calibration/validation studies of URM buildings to overcome the global rigidity given by local connections which results in over stiff results. An overview of the parameters employed in the material model is shown in Table 3. The NLTH material properties for the elastic parameters are included in parenthesis.

Table 3. Masonry properties numerical model. In parenthesis the values used for the NLTHA.

Engineering Masonry Model	**CaSi**	**CaSi – Weak***
E_y [MPa]	4000 (2000)	2800 (1400)
E_x [MPa]	2667 (1334)	1867 (934)
G [MPa]	1650 (825)	1155 (578)
Density [Kg/m^3]	1850	1850
f_y [MPa]	0.15	0.10
Min f_x [MPa]	0.30	0.20
$G_{f,I}$ [N/m]	10	8.1
α [rad]	0.62	0.62
f_c [MPa]	7.0	7.0
G_c [N/m]	15000	15000
φ [rad]	0.54	0.57
c [MPa]	0.25	0.175
G_s [N/m]	100	100

* Rotated local axis

2.3.2 Timber Planks

An orthotropic behaviour, whose properties are calibrated according to past laboratory experiment, is assigned to timber planks of the roof. The local axes are aligned to the global ones. The properties are tabulated in Table 4.

Table 4. Roof timber diaphragm properties numerical model.

Linear Elastic Orthotropic	Timber C18 - Plates
E_x [MPa]	1.5
E_y [MPa]	11
E_z [MPa]	400
Density [Kg/m³]	380
υ [-]	0.15
G_{xy} [MPa]	1100
G_{yz} [MPa]	1100
G_{xz} [MPa]	500

2.3.3 Timber Beams and Dummy Beams

Beam properties are considered as isotropic linear elastic. The material assigned to purlins, ridge, struts, ties and to the dummy beams along the perimeters of the roof diaphragm are listed in Table 5.

Table 5. Timber and dummy beam properties numerical model.

Linear Elastic Isotropic	Timber C18	Dummy
E [MPa]	9000	1000
Density [Kg/m³]	380	-
υ [-]	0.35	0.35

2.3.4 Gable-Beams Interfaces

The Coulomb-Friction model is used for the point interface between gables and purlin beams of the roof. The material properties are shown in Table 6.

Table 6. Gable-Purlin interface properties numerical model.

Coulomb Friction Interface	Gable-Purlin Connection
k_n [N/mm³]	1000
k_t [N/mm³]	100
φ [rad]	0.60
Ψ [rad]	0
c [MPa]	0.02
f_t [MPa]	No open

2.3.5 Reinforced Concrete

Floor material is modelled as non-linear using the Total Strain Rotating Crack Model for the concrete and the Von Mises plasticity for the rebar. The properties are listed in Table 7 and Table 8.

Table 7. Reinforced concrete properties numerical model.

Total Strain Rotating Crack Model	C20/25
E [MPa]	27088

Density [Kg/m³]	2500
υ [-]	0.15
f_t [MPa]	1.55
$G_{f,I}$ [N/m]	125
f_c [MPa]	20.0
G_c [N/m]	31293

Table 8. Rebar properties numerical model.

Von Mises Plasticity	Fe400
E [MPa]	200000
f_y [MPa]	400

2.4 Interstorey and Effective Heights

The interstorey height and the effective height are shown in Figure 11. The calculation of the effective height, as well as of the effective mass is evaluated following the recommendation of Annex G of NPR. These values are then used for the drift calculations. The effective heights and effective masses evaluated in the different model is shown in Table 9. The transformation factor is also included.

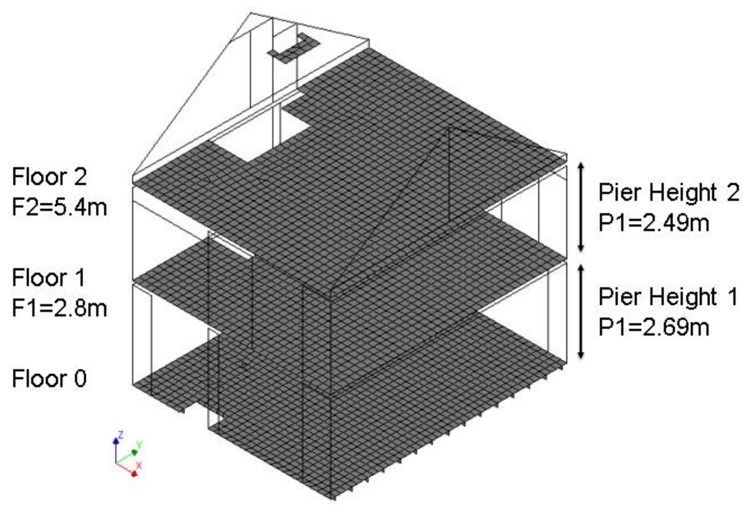

Figure 11. Floor height definitions.

Table 9. Effective heights, effective masses and transformation factor for different models.

Models	Effective Height [m]	Effective Mass [ton]	Transformation Factor Γ
Modal - Positive X	4.968	207.3 (69.1 per unit)	1.087
Modal - Negative X	5.005	209.1 (69.7 per unit)	1.079
Uniform - Positive X	5.017	209.7 (69.9 per unit)	1.076
Uniform - Negative X	5.032	210.6 (70.2 per unit)	1.073

2.5 Vertical Loads

The floor weights and the non-structural mass are given in Table 10.

Table 10. Floor weights and non-structural mass.

Models	Dead Load [kN/m²]	Superimposed Dead Load [kN/m²]	Live Load [kN/m²]	Comments
Ground – Kwaaitaal Floor	2.37	1.00	0.315	50 mm screed
Storey 1 – Concrete Slab	2.67	0.80	0.315	40 mm screed
Storey 2 – Concrete Slab	2.67	0.80	0.315	40 mm screed
Roof – Purlins, Trusses, Concrete Tiles	0.099	0.50	0.000	Concrete Tiles (0.5 kN/m²)

2.6 Mass and Vertical Reaction

The static and dynamic mass for each floor is listed in Table 11. The dynamic mass includes the mass of veneers, chimney and extra-floor-mass, as specified in Section 2.5.

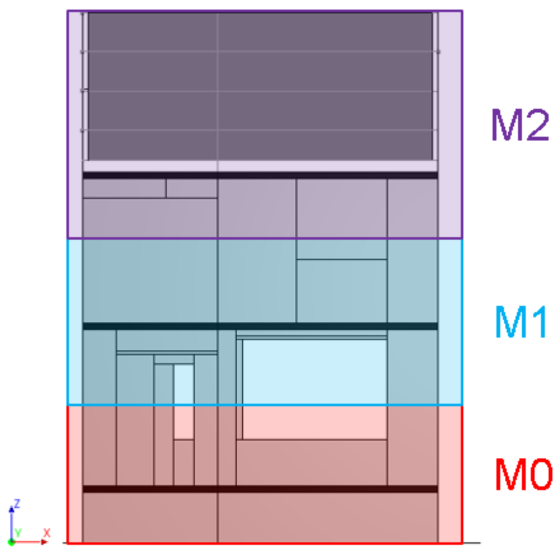

Figure 12. Mass division to the different storeys.

Table 11. Static and Dynamic Masses per each storey.

Mass	Static Mass [ton]	Dynamic Mass [ton]
M0	86.1 (28.7 per unit)	108.6 (36.2 per unit)
M1	91.8 (30.6 per unit)	113.4 (37.8 per unit)
M2	89.4 (29.8 per unit)	114.0 (38.0 per unit)
Mtot	**267.3 (89.1 per unit)**	**336.0 (112.0 per unit)**

The total vertical reaction force is equal to 87400 kN corresponding to a total mass of 89.1 tons for the static mass. The dynamic mass accounted in the model is equal to 112.0 tons.

2.7 Element labelling

Piers, window banks and spandrels are labelled in order to assess their local behaviour in terms of load and displacement capacity. The name configuration consists of:

- A letter to indicate the element location: F for longitudinal front façade, B for longitudinal back façade, L for transversal left façade, R for transversal right façade, I for internal wall (either longitudinal or transversal).
- A letter to indicate the element type: P for pier, B for bank and S for spandrel.
- A number defining the level of the element: 1 for the element located between ground and first storey and 2 for the element located between first and attic storey level.
- A progressive number to univocally identify a specific element.

An overview of the labelling is shown in Figure 13 for piers and in Figure 14 for window banks and spandrels.

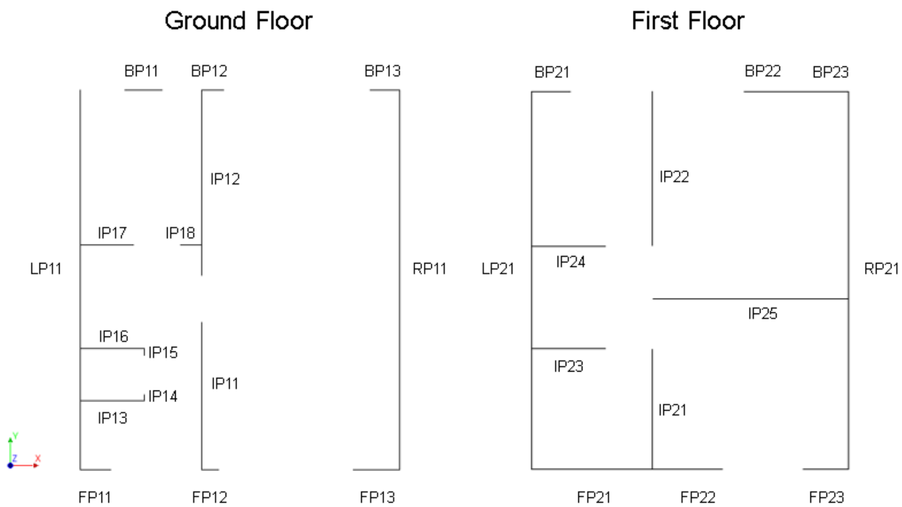

Figure 13. Pier labelling for ground and first floor.

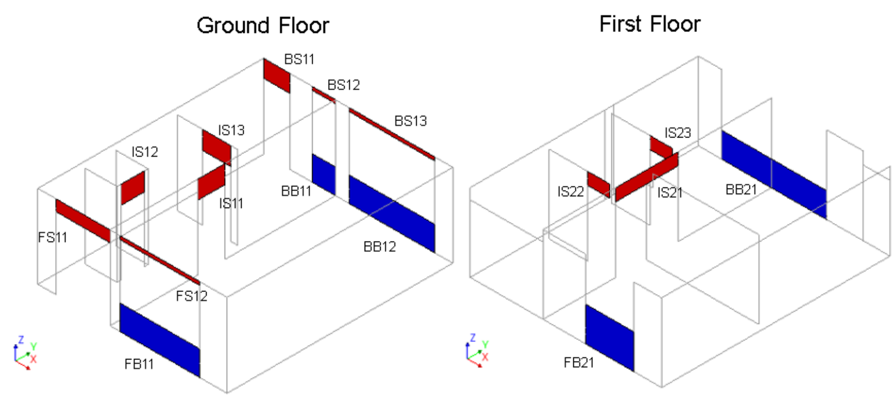

Figure 14. Banks and Spandrel labelling for ground and first floor.

2.8 Unknown Information and Modelling Assumptions

The model is based on the following assumptions/limitations:

- No structural drawings were available;
- Only one building unit is modelled.
- The appendixes are not modelled;
- No interaction between the building unit and the appendix, nor between the units is assumed;
- The veneer (outer leaves) and the chimney are not modelled explicitly, rather as dynamic mass acting in the direction perpendicular to the wall;

- The connection between longitudinal and transversal walls (load-bearing) is consider as interlocked, thus either translations and rotations are fully transferred at the connection;
- The connection between internal non-load bearing walls and load-bearing walls is assumed as weak connection, assigning low material properties to a strip of elements along the connection;
- No connection is considered between the internal non-load bearing walls and the floor above them;
- The connection between floors and walls is considered as fully fixed (translations and rotations are transferred);
- Interfaces with Coulomb-friction criteria are used to model the connection between purlins/ridge beams and the gables.

3 NLPO ANALYSES

3.1 NLPO Assessment

Building B is assessed via Non-Linear Pushover Analyses with Diana FEA 10.3. Both uniform and modal distributed load analyses are performed. The former is applied via an equivalent acceleration to the entire structure. The latter is based on the main eigen-mode and the forces are automatically applied in order to follow the deformed shape of the natural mode. The main mode is shown in Figure 15. The main eigen-frequency is equal to 3.7849 Hz which gives a period of 0.264 s. No main mode is evaluated in the global y direction.

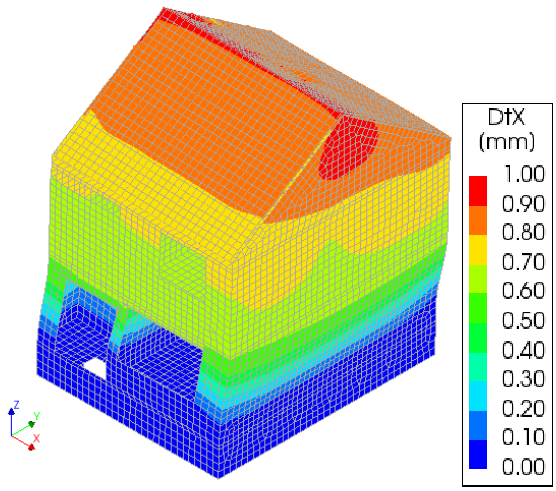

Figure 15. First natural mode of Building B. Longitudinal displacement plot.

3.2 Global Results

3.2.1 Failure Mechanisms

The failure mechanisms of the different analyses are reported below. The failure mechanism in all cases is clearly related to a soft-storey mechanism at the ground storey level. The type of failure can be considered as flexural failure of the piers, therefore for each storey may consider the ductile storey drift limit of 1.5%.

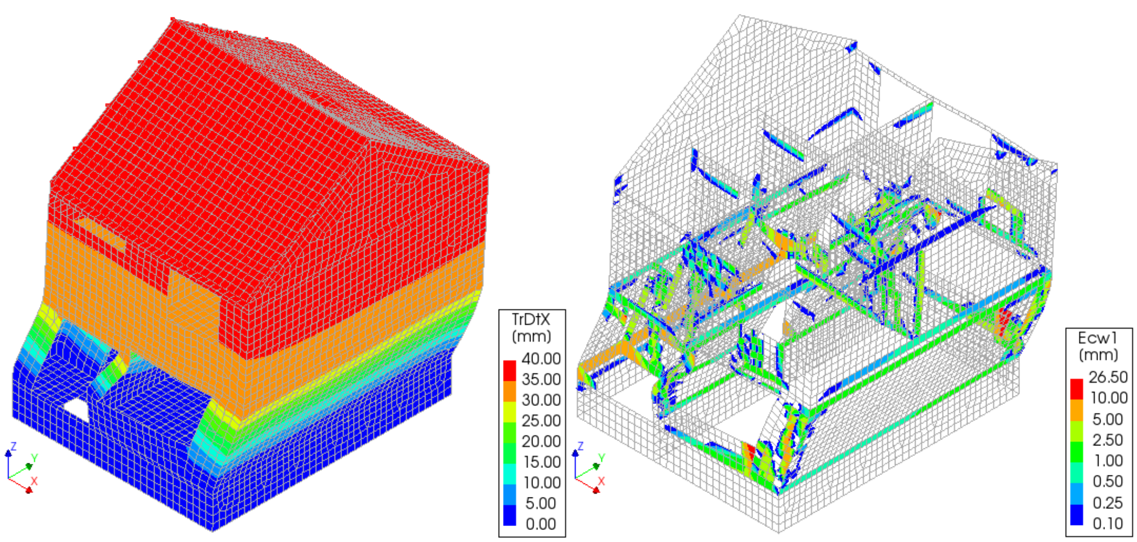

Figure 16. Modal Distribution Positive X direction. Longitudinal displacement and principal crack width at step 385.

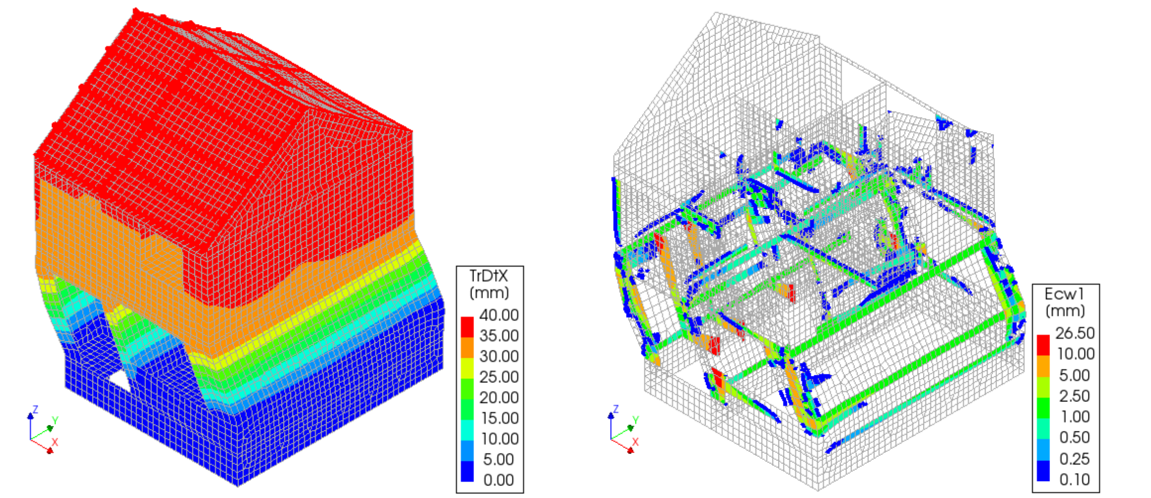

Figure 17. Modal Distribution Negative X direction. Longitudinal displacement and principal crack width at step 385.

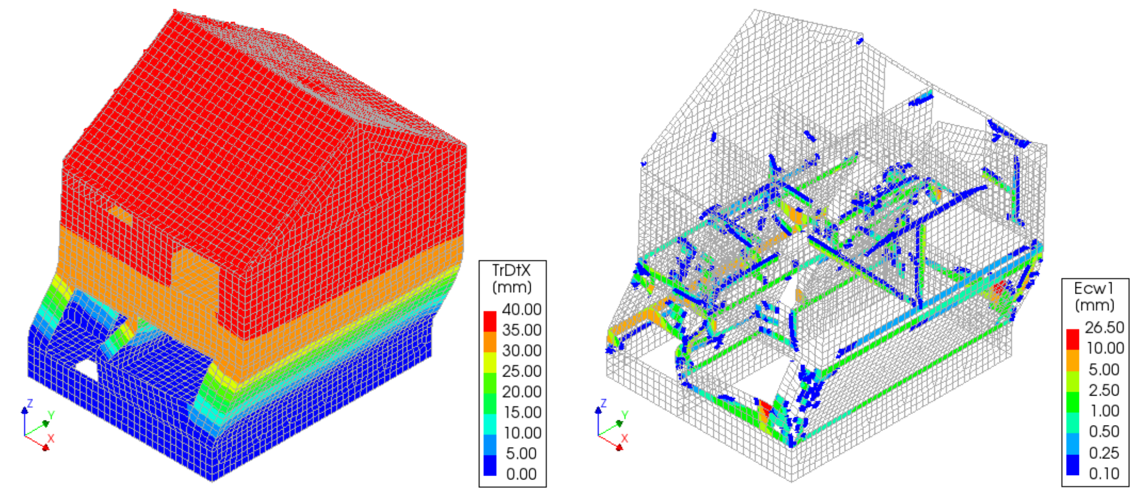

Figure 18. Uniform Distribution Positive X direction. Longitudinal displacement and principal crack width at step 385.

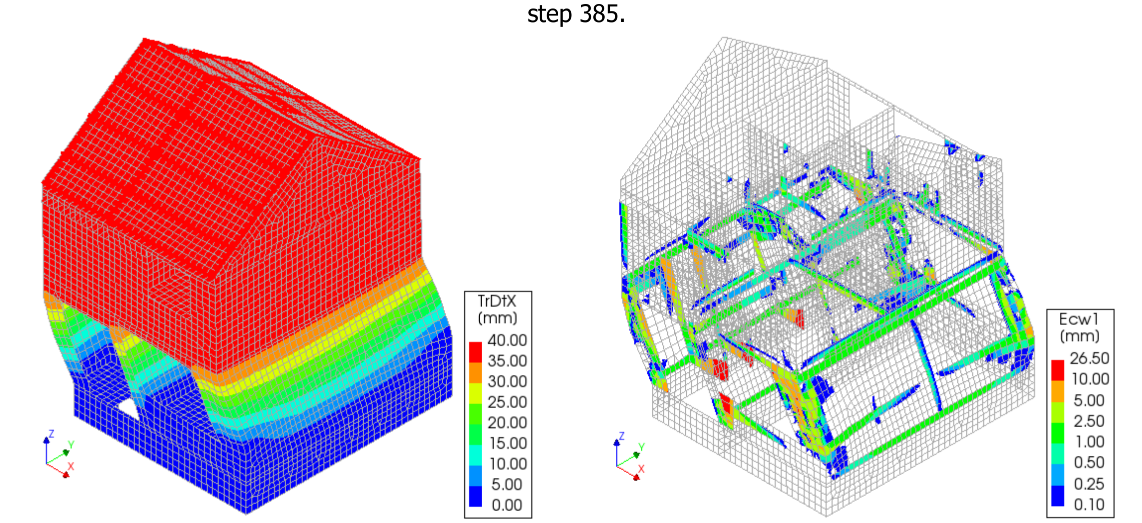

Figure 19. Uniform Distribution Negative X direction. Longitudinal displacement and principal crack width at step 385.

3.2.2 Capacity Curves

The force-displacement and acceleration-displacement diagrams for the different analyses are shown from Figure 20 to Figure 23. The vertical yellow line refers to the 1.5% drift limit of the ground floor. The acceleration is computed dividing the force by the effective mass. Figure 24 shows the comparison between the different pushover analyses. The force-displacement curves are then bilinearized following the procedure recommended in section G.4 and shown in Figure 25. The main results of both multilinear athe nd bilinearized pushover curves are tabulated in Table 12 and Table 13.

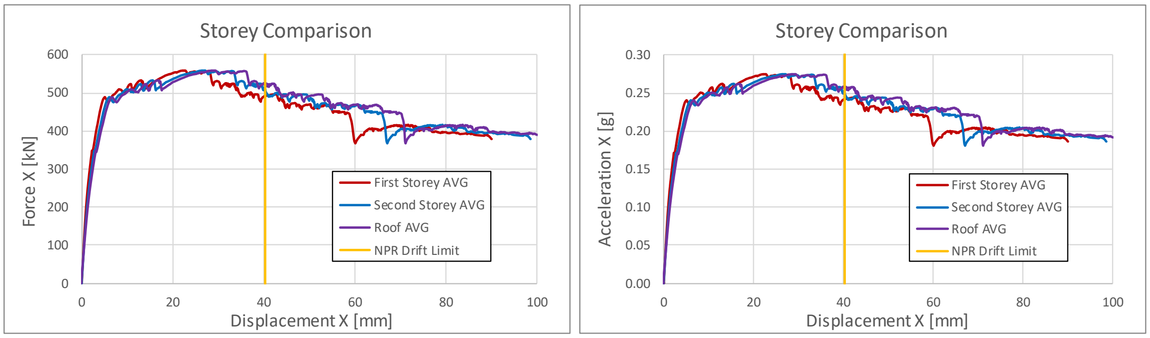

Figure 20. Modal Distribution Positive X direction. Storey comparison. Capacity per unit: 186.36 kN.

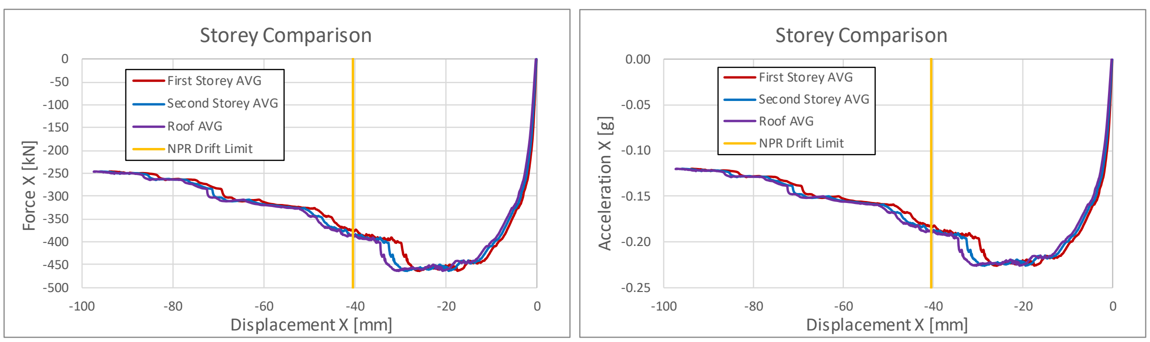

Figure 21. Modal Distribution Negative X direction. Storey comparison. Capacity per unit: -154.78 kN.

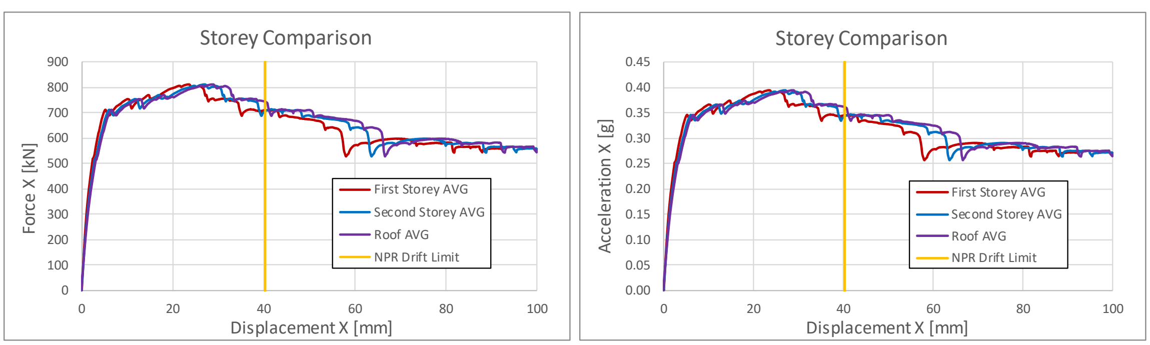

Figure 22. Uniform Distribution Positive X direction. Storey comparison. Capacity per unit: 270.78 kN.

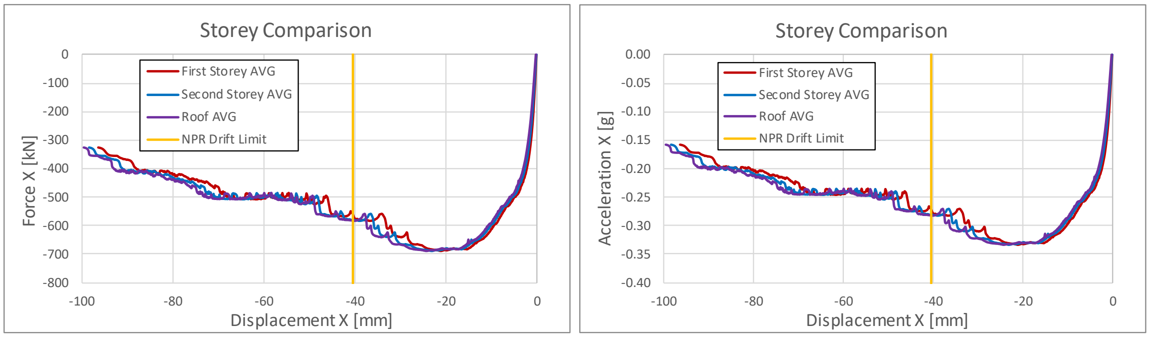

Figure 23. Uniform Distribution Negative X direction. Storey comparison. Capacity per unit: -229.78 kN.

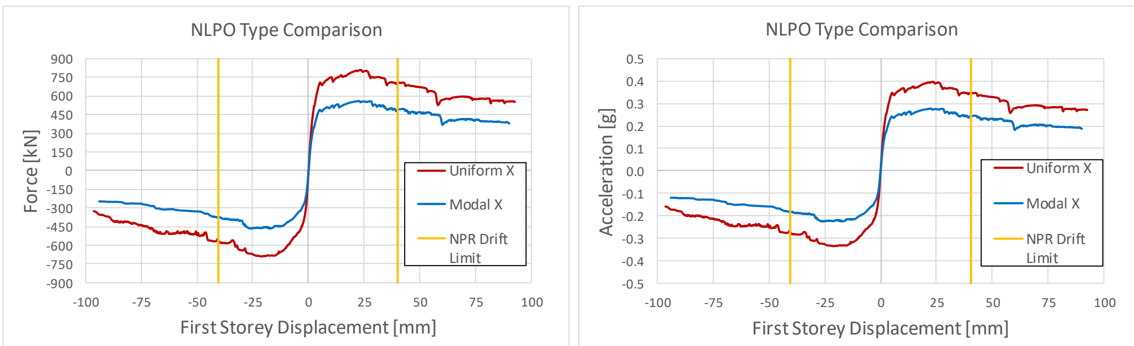

Figure 24. NLPO comparison. Force/Acceleration vs First floor displacement.

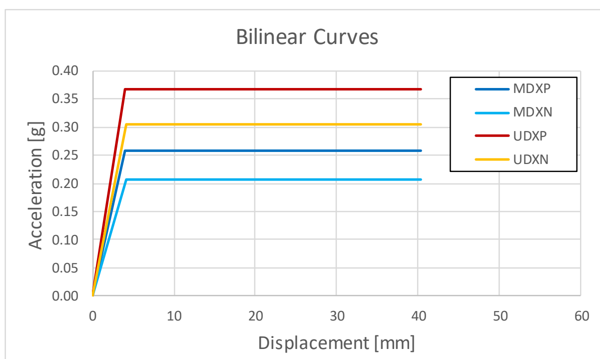

Figure 25. NLPO comparison. Bilinear Curves.

Table 12. Global NLPO Results.

Models	Governing Failure	Capacity [kN]	Acceleration [g]	Displacement First Floor [mm]
Modal - Positive X	Flexure	559.1 (186.4 per unit)	0.275	40.41
Modal - Negative X	Flexure	464.4 (154.8 per unit)	0.226	40.42
Uniform - Positive X	Flexure	812.4 (270.8 per unit)	0.395	40.37
Uniform - Negative X	Flexure	689.4 (229.8 per unit)	0.333	40.35

Table 13. Global NLPO Results – Bilinearized Curves.

Models	Yield Displacement [mm]	Displacement Capacity [mm]	Acceleration [g]
Modal - Positive X	4.02	40.35	0.259
Modal - Negative X	4.21	40.35	0.207
Uniform - Positive X	4.00	40.35	0.367
Uniform - Negative X	4.10	40.35	0.306

3.2.3 Inter-storey Drifts

Inter-storey drift displacements are expressed in terms of drifts in Table 14.

Table 14. NLPO inter-storey drifts.

Models	Inter-storey drift Floor 1 [-]	Inter-storey drift Floor 2 [-]
Modal - Positive X	40.41 mm / 1.50 %	6.43 mm / 0.26 %
Modal - Negative X	40.42 mm / 1.50 %	2.32 mm / 0.09 %
Uniform - Positive X	40.37 mm / 1.50 %	4.87 mm / 0.20 %
Uniform - Negative X	40.35 mm / 1.50 %	2.24 mm / 0.09 %

3.2.4 Assessment

The assessment of the four NLPO analyses is made following the procedure described in Annex G of NPR. Both uniform and modal distributed pushover met the seismic demand for the elastic ADRS. The former ones met the elastic capacity demand, while the latter ones met the elastic displacement demand. An overview of the elastic spectrum is depicted in Figure 26. The elastic spectrum is scaled to the non-linear ADRS for the two modal pushover analyses. The plot showing the performance points is shown in Figure 26. Values of global ductility and equivalent viscous damping are listed in Table 15.

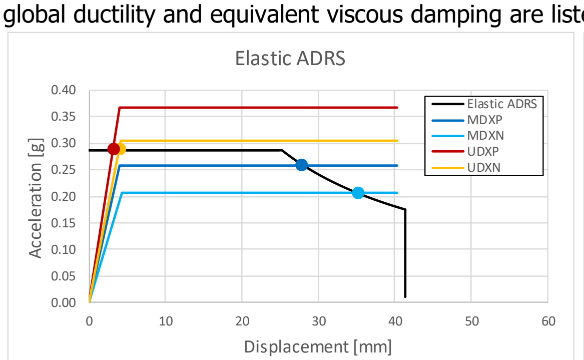

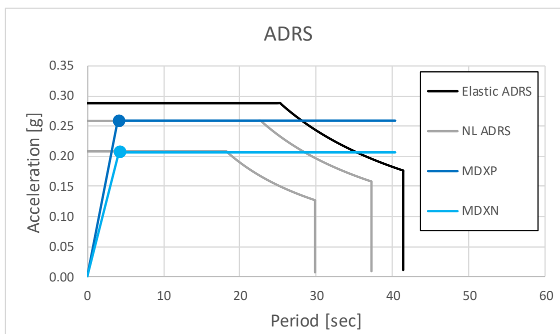

Figure 26. NLPO assessment. Elastic (left) and non-linear (right) ADRS for site-specific hazard.

Table 15. Modal NLPO equivalent damping and global ductility for non-linear ADRS ADRS for site-specific hazard.

Models	Equivalent Damping ξ_{sys}	Global Ductility μ_{sys}
Modal - Positive X	6.68%	1.108
Modal - Negative X	11.48%	1.559

The site-specific PGA is then scaled in order to satisfy the displacement demand of the modal pushover analyses for the non-linear ADRS. The iterated PGA of the pushover in the positive direction is equal to 0.305

g, while for the negative direction is 0.275 g. The scaled ADRS plots together with the performance points are represented in Figure 27. In Table 16, the scaled PGA, global ductility and equivalent viscous damping are listed.

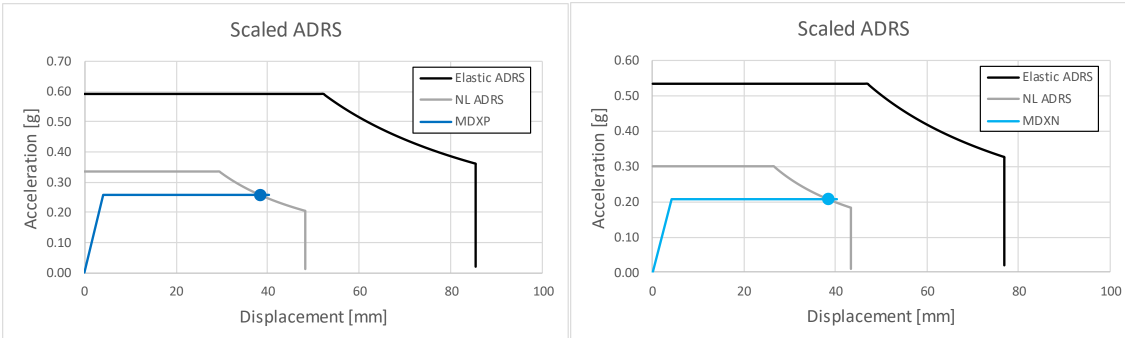

Figure 27. NLPO assessment modal pushover. Scaled ADRS for positive load direction (left) and negative load direction (right).

Table 16. Modal NLPO equivalent damping and global ductility for non-linear ADRS ADRS for site-specific hazard.

Models	Scaled Acceleration [g]	Equivalent Damping ξ_{sys}	Global Ductility μ_{sys}
Modal - Positive X	0.305	20.00%	10.04
Modal - Negative X	0.275	20.00%	9.59

3.3 Results for the individual elements

In order to evaluate the local behaviour of piers, banks and spandrels, the force contribution and the drift at global peak of the analysis are extrapolated and reported. The data is taken from the modal pushover analysis with negative direction (having the lowest capacity). The elements are labelled as presented in Section 2.7.

3.3.1 Pier Force and Drift

The force contribution and drift of piers are listed in Table 17. The drift progression of the piers on the front and back façades is plotted in Figure 28. The drift limit of the single piers are also plotted (the calculation follows formula G.31 of Annex G of NPR): the global drift limit of the structure is reached before that any of the piers reach its local drift limit.

Table 17. Pier force and drift at the peak of modal pushover negative x direction.

Pier	Effective Height [mm]	Displacement at peak [mm]	Drift at peak	Force X at Peak [kN]	Force contribution at Peak
BP11	2690	-25.50	-0.95%	-25.21	16.29%
BP12	1890	-25.55	-1.35%	-4.56	2.95%
BP13	1890	-25.37	-1.34%	7.64	-4.94%
BP21	2490	-2.66	-0.11%	-10.20	6.59%
BP22	2490	-2.72	-0.11%	6.26	-4.04%
BP23	2100	-1.97	-0.09%	16.93	-10.94%
FP11	2690	-25.34	-0.94%	-13.34	8.62%
FP12	2690	-25.43	-0.95%	-13.33	8.61%

FP13	1890	-25.36	-1.34%	30.34	-19.60%
FP21	2150	-0.65	-0.03%	-28.43	18.37%
FP22	2490	-2.61	-0.10%	-12.20	7.88%
FP23	2490	-2.56	-0.10%	35.21	-22.75%
IP11	2690	-25.49	-0.95%	-4.42	2.86%
IP12	2690	-25.55	-0.95%	12.24	-7.91%
IP13	2690	-19.15	-0.71%	-4.39	2.84%
IP14	2690	-18.27	-0.68%	-0.23	0.15%
IP15	2690	-18.27	-0.68%	-0.23	0.15%
IP16	2690	-19.06	-0.71%	-4.32	2.79%
IP17	2690	-26.31	-0.98%	-22.13	14.30%
IP18	2690	-25.13	-0.93%	4.18	-2.70%
IP21	2490	-2.64	-0.11%	10.01	-6.47%
IP22	2490	-2.77	-0.11%	-2.28	1.47%
IP23	2490	-2.78	-0.11%	-11.27	7.28%
IP24	2490	-3.22	-0.13%	-6.33	4.09%
IP25	2490	-1.97	-0.08%	-17.52	11.32%
LG31	2750	-1.90	-0.07%	-2.74	1.77%
LP11	2690	-25.59	-0.95%	-20.43	13.20%
LP21	2490	-2.68	-0.11%	-8.15	5.27%
RG31	2750	-1.72	-0.06%	3.29	-2.13%
RP11	2690	-25.39	-0.94%	22.22	-14.36%
RP21	2490	-2.52	-0.10%	19.34	-12.50%

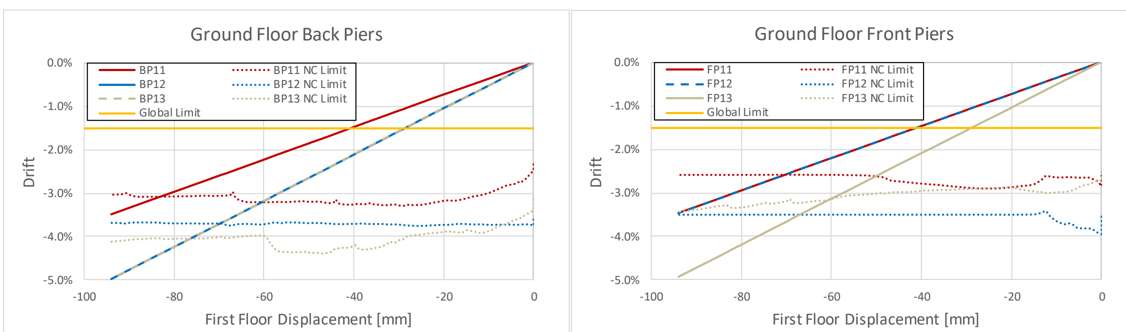

Figure 28. Drift progression of front and back piers of the modal pushover negative x direction.

3.3.2 Bank-Spandrel Force and Drift

Force contribution and drift of banks and spandrels are listed in Table 19. Reduced drifts (below the limit of 2%) are found for every element.

Table 18. Bank and spandrel force and drift at the peak of modal pushover negative x direction.

Bank - Spandrel	Effective Height [mm]	Displacement at peak [mm]	Drift at peak	Force X at Peak [kN]	Force contribution at Peak
BB11	800	-2.03	-0.25%	-1.43	0.92%
BB12	800	0.10	0.01%	-21.46	13.86%
BB21	800	-0.57	-0.07%	-15.92	10.29%
BS11	560	0.14	0.03%	-4.81	3.11%
BS12	110	-0.13	-0.12%	1.45	-0.94%

BS13	110	0.04	0.03%	0.47	-0.31%
FB11	800	0.11	0.01%	-21.55	13.92%
FB21	1100	-0.54	-0.05%	-7.23	4.67%
FS11	360	-0.08	-0.02%	13.30	-8.59%
FS12	110	0.00	0.00%	1.96	-1.27%
IS11	590	-3.81	-0.65%	-0.87	0.57%
IS12	590	-4.15	-0.70%	0.00	0.00%
IS13	590	-2.96	-0.50%	-10.38	6.70%
IS21	390	0.05	0.01%	1.97	-1.27%
IS22	390	0.19	0.05%	-0.07	0.05%
IS23	390	0.32	0.08%	-0.71	0.46%

4 NLTH ANALYSES

4.1 NPR Assessment For Site-Specific Hazard – Indirect Method

The site-specific hazard is assessed using the indirect method as defined in section F.6.3 of NPR. The ground motions input is described in Section 2.2. Overall, the Building B complies with NPR.
The average maximum displacement in x-direction recorded at the first floor location is 8.23 mm, equal to 0.31% of the effective height. The displacement in the y direction is small, 0.54 mm at the first floor level. The average peak forces are equal to 427 kN in the positive direction and 395 kN for the negative direction in x. For the y direction the maximum forces in positive and negative direction are 484 kN and 492 kN.

4.1.1 Failure Mechanisms

The observed failure mechanism is a soft-storey mechanism located at the ground storey level. The ductile storey drift limit of 1.5% is considered. An example of failure mechanism is reported below in Figure 29.

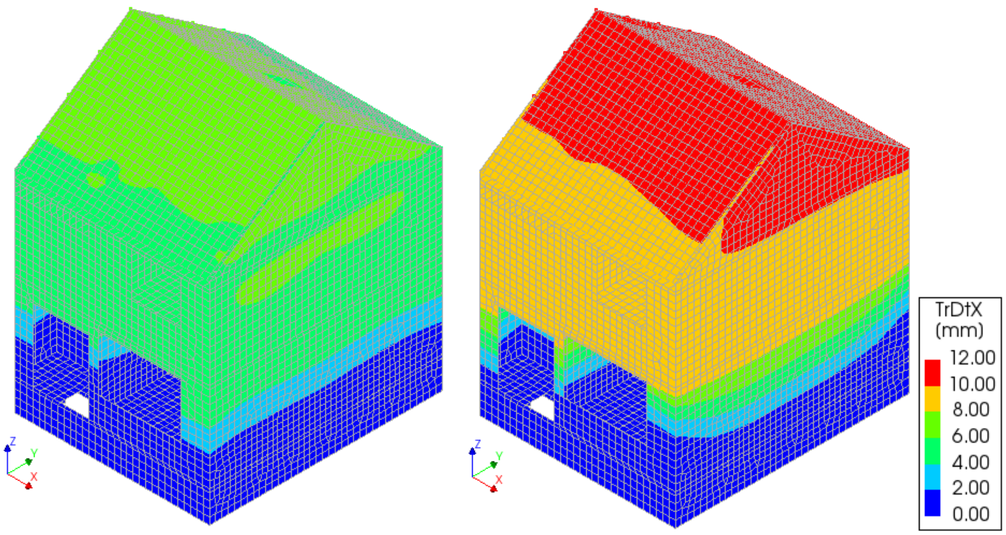

Figure 29. GM ID 5 for site-specific hazard. Absolute maximum (left) and minimum (right) longitudinal displacement recorded during the entire motion.

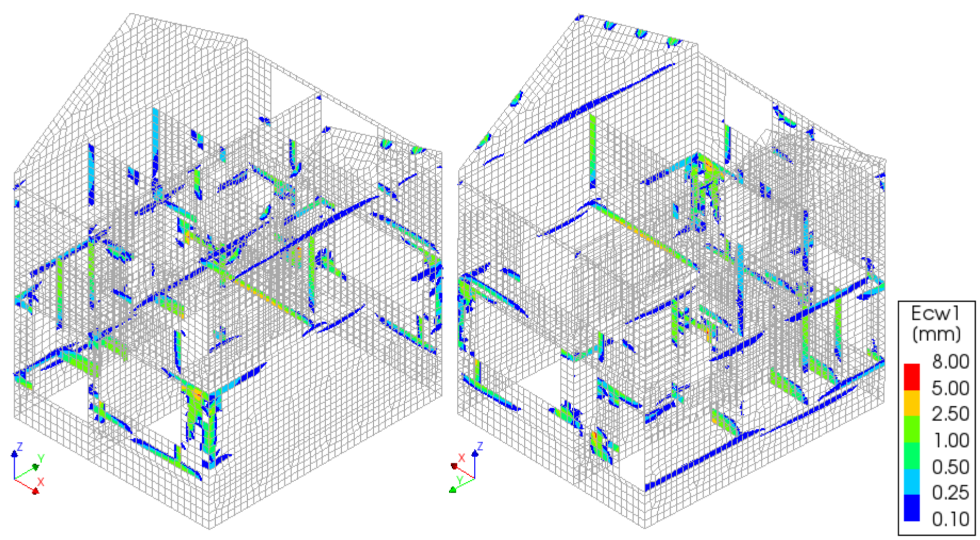

Figure 30. GM ID 5 for site-specific hazard. Absolute maximum principal crack width recorded during the entire motion. Front (left) and back(right) view.

4.1.2 Inter-storey Drifts

The peak values of Inter-storey displacements and drifts for both x and y directions are reported in Table 19 and Table 20.

Table 19. Inter-storey displacement NLTHA results for site-specific hazard.

GM ID	Peak Displacement X Direction - mm			Peak Displacement Y Direction - mm		
	Floor 1	Floor 2	Floor 3	Floor 1	Floor 2	Floor 3
1	5.91	1.08	0.80	0.53	0.42	0.33
2	9.08	1.23	0.89	0.52	0.39	0.26
3	9.41	1.09	0.85	0.48	0.37	0.27
4	8.56	1.08	0.84	0.56	0.40	0.32
5	8.99	1.08	0.72	0.44	0.38	0.27
6	10.15	1.32	0.93	0.46	0.41	0.33
7	8.01	1.29	0.92	0.59	0.49	0.35
8	5.89	1.19	0.82	0.53	0.41	0.34
9	8.51	1.14	0.92	0.49	0.35	0.27
10	9.91	1.17	1.07	0.58	0.44	0.33
11	6.14	1.33	0.80	0.80	0.61	0.47
Mean	**8.23**	**1.18**	**0.87**	**0.54**	**0.42**	**0.32**

Table 20. Inter-storey drift NLTHA results for site-specific hazard.

GM ID	Peak Drift X Direction - %			Peak Drift Y Direction - %		
	Floor 1	Floor 2	Floor 3	Floor 1	Floor 2	Floor 3
1	0.22	0.04	0.03	0.02	0.02	0.01
2	0.34	0.05	0.03	0.02	0.02	0.01
3	0.35	0.04	0.03	0.02	0.01	0.01
4	0.32	0.04	0.03	0.02	0.02	0.01
5	0.33	0.04	0.03	0.02	0.02	0.01
6	0.38	0.05	0.03	0.02	0.02	0.01
7	0.30	0.05	0.03	0.02	0.02	0.01
8	0.22	0.05	0.03	0.02	0.02	0.01
9	0.32	0.05	0.03	0.02	0.01	0.01
10	0.37	0.05	0.04	0.02	0.02	0.01
11	0.23	0.05	0.03	0.03	0.02	0.02
Mean	**0.31**	**0.05**	**0.03**	**0.02**	**0.02**	**0.01**

4.1.3 Effective Height Drifts

The maximum drifts evaluated at the effective height of the building are listed for both the x- and y-direction in Table 21.

Table 21. Peak effective height drift for NLTHA analyses for site-specific hazard.

GM ID	Peak Effective Height Drift X [%]	Peak Effective Height Drift Y [%]
1	0.11	0.01
2	0.16	0.01
3	0.17	0.01
4	0.15	0.02
5	0.16	0.01
6	0.18	0.01
7	0.14	0.02
8	0.11	0.01
9	0.15	0.01
10	0.17	0.02
11	0.12	0.02
Mean	**0.15**	**0.01**

4.1.4 Base Shear

Maximum reached base shear for both x and y direction is reported in Table 22. The governing mechanism is a ductile mechanism at the ground-floor.

Table 22. Base shear NLTHA results for site-specific hazard.

GM ID	Governing Failure	Base Shear X [kN]	Base Shear Y [kN]
1	Flexure	+468.67 / -337.77	+464.36 / -477.15
2	Flexure	+506.53 / -431.55	+411.05 / -554.52
3	Flexure	+353.01 / -415.73	+436.80 / -491.04
4	Flexure	+410.93 / -408.62	+498.96 / -499.98
5	Flexure	+430.10 / -362.28	+472.64 / -428.93
6	Flexure	+386.34 / -425.06	+418.77 / -430.90
7	Flexure	+467.70 / -365.55	+481.90 / -560.86
8	Flexure	+429.42 / -370.51	+440.66 / -494.14
9	Flexure	+380.95 / -474.70	+483.68 / -442.44
10	Flexure	+367.59 / -421.04	+440.40 / -515.93
11	Flexure	+496.93 / -332.86	+773.36 / -516.39
Mean		**+427.11 / -395.06**	**+483.87 / -492.03**

4.1.5 Pier Shear Forces

The force contribution and the drift of piers at the global peak force for each of the two directions are listed in Table 23 and Table 24.

Table 23. Pier force and drift at the peak of GM ID 5 site-response hazard in x direction.

Pier	Effective Height [mm]	Displacement at peak [mm]	Drift at peak	Force X at Peak [kN]	Force contribution at Peak
BP11	2690	4.24	0.16%	4.42	3.09%
BP12	1890	4.25	0.22%	0.32	0.22%
BP13	1890	4.22	0.22%	3.48	2.43%
BP21	2490	0.80	0.03%	2.26	1.58%
BP22	2490	0.80	0.03%	-1.47	-1.02%
BP23	2100	0.50	0.02%	-3.40	-2.37%
FP11	2690	4.11	0.15%	5.86	4.09%
FP12	2690	4.14	0.15%	3.05	2.13%
FP13	1890	4.08	0.22%	13.68	9.54%
FP21	2150	0.52	0.02%	-2.33	-1.63%
FP22	2490	0.80	0.03%	-18.79	-13.11%
FP23	2490	0.82	0.03%	-6.77	-4.73%
IP11	2690	4.15	0.15%	1.75	1.22%
IP12	2690	4.21	0.16%	2.15	1.50%
IP13	2690	3.96	0.15%	7.54	5.26%
IP14	2690	3.89	0.14%	1.21	0.84%
IP15	2690	3.89	0.14%	1.21	0.84%
IP16	2690	3.92	0.15%	7.22	5.04%
IP17	2690	3.58	0.13%	7.34	5.12%
IP18	2690	3.72	0.14%	2.51	1.75%
IP21	2490	0.79	0.03%	1.10	0.77%
IP22	2490	0.79	0.03%	1.27	0.89%
IP23	2490	0.81	0.03%	1.85	1.29%
IP24	2490	0.87	0.04%	0.92	0.64%
IP25	2490	0.10	0.00%	8.61	6.00%
LG31	2750	0.49	0.02%	2.27	1.58%
LP11	2690	4.05	0.15%	-18.27	-12.74%
LP21	2490	0.92	0.04%	-0.88	-0.61%
RG31	2750	0.58	0.02%	6.83	4.76%
RP11	2690	4.24	0.16%	11.33	7.91%
RP21	2490	0.91	0.04%	6.84	4.77%

Table 24. Pier force and drift at the peak of GM ID 5 site-response hazard in y direction.

Pier	Effective Height [mm]	Displacement at peak [mm]	Drift at peak	Force Y at Peak [kN]	Force contribution at Peak
BP11	2690	0.36	0.01%	0.32	0.20%
BP12	1890	0.37	0.02%	0.34	0.22%
BP13	1890	0.36	0.02%	0.71	0.45%
BP21	2490	0.29	0.01%	0.04	0.03%
BP22	2490	0.47	0.02%	1.01	0.64%
BP23	2100	0.52	0.02%	0.43	0.27%
FP11	2690	0.30	0.01%	-0.14	-0.09%

FP12	2690	0.32	0.01%	0.09	0.06%
FP13	1890	0.35	0.02%	-0.32	-0.20%
FP21	2150	0.61	0.03%	0.36	0.23%
FP22	2490	0.32	0.01%	0.77	0.49%
FP23	2490	0.40	0.02%	0.48	0.31%
IP11	2690	0.33	0.01%	6.37	4.04%
IP12	2690	0.35	0.01%	6.59	4.18%
IP13	2690	0.64	0.02%	0.17	0.11%
IP14	2690	0.92	0.03%	0.04	0.03%

4.1.6 Capacity Curves

The force-displacement curve of each ground motion are depicted in Figure 31. The displacement is recorded at the effective height location.

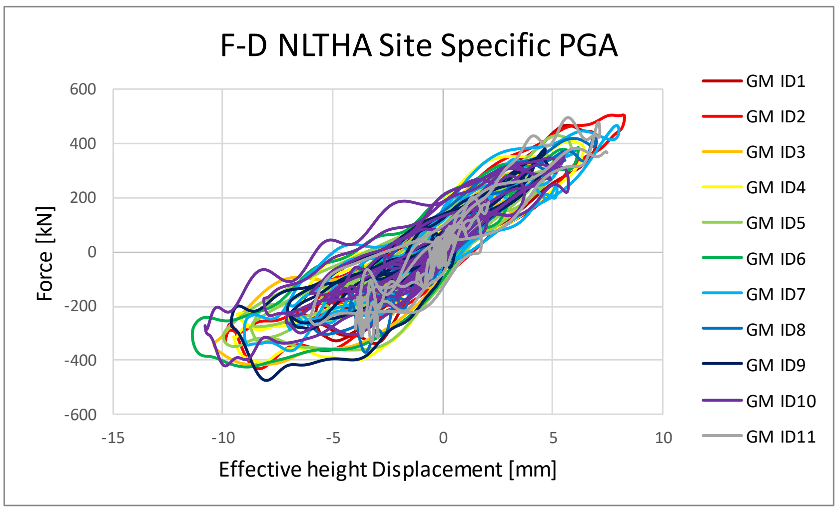

Figure 31. Capacity curves of each ground motion for site-specific hazard.

4.2 Iterative Scaling of Input Ground Motion – Indirect Method

The original ground motions are amplified in order to evaluate the peak ground acceleration (PGA) that leads to failure (exceedance of the global drift limits), following an indirect method. The ground motions are scaled to a PGA of 0.33g.

The global mechanism is a soft-storey at the ground floor along the weak x direction. The average maximum displacement in x direction recorded at the first floor location is 35.5 mm, equal to 1.32% of global drift. The average drift is below the drift limit calculated from normative. Considering the results of extra calculations with an higher PGA, the failure (i.e. the exceedance of the 1.5% interstorey drift) is expected for ground motions scaled up with a PGA between 0.35g and 0.40g. The displacements in the y direction are relatively small, and at the first floor level equals to 1.54 mm. Average peak forces are equal to 646 kN in the positive direction and 630 kN for the negative direction in x. For the y direction the maximum forces in positive and negative direction are 1032kN and 952 kN.

4.2.1 Failure Mechanisms

The observed failure mechanism is a soft-storey mechanism located at the ground floor. The ductile storey drift limit of 1.5% is considered. An example of failure mechanisms is shown below in Figure 32.

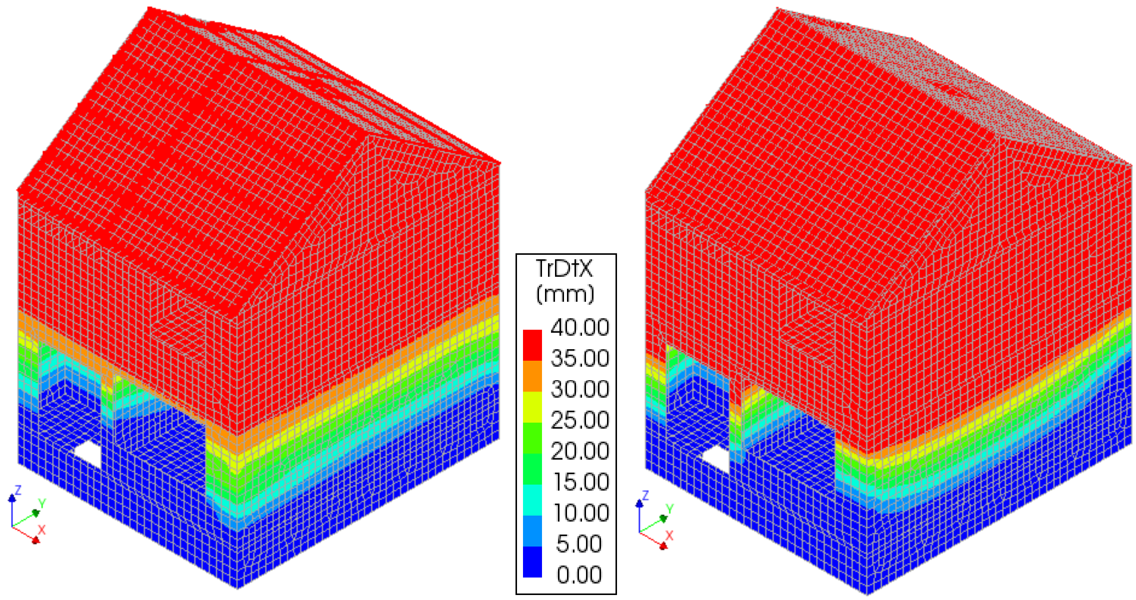

Figure 32. GM ID 8 for iterated PGA. Absolute maximum (left) and minimum (right) longitudinal displacement recorded during the entire motion.

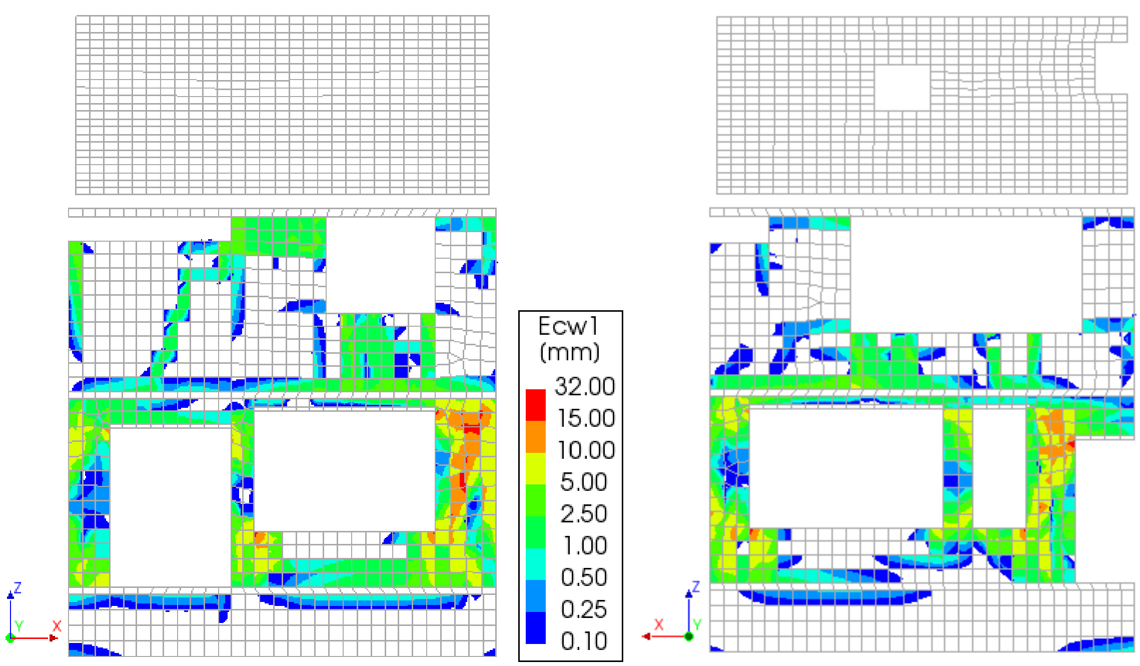

Figure 33. GM ID 8 for iterated PGA. Absolute maximum principal crack width recorded during the entire motion. Front (left) and back(right) façade.

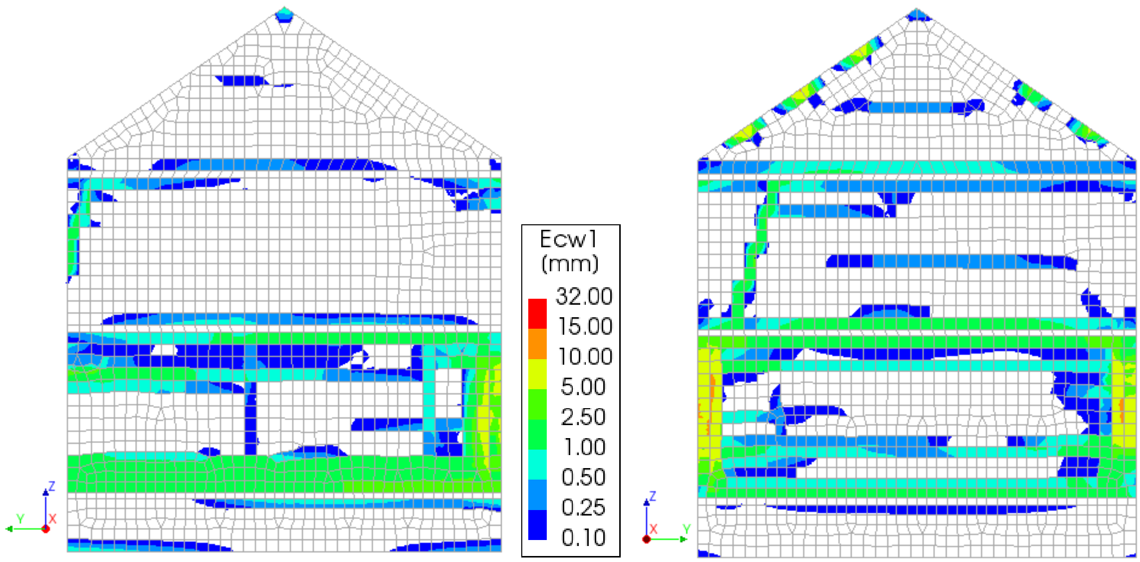

Figure 34. GM ID 8 for iterated PGA. Absolute maximum principal crack width recorded during the entire motion. Left (left) and right (right) façade.

4.2.2 Inter-storey Drifts

The peak values of the inter-storey displacements and drifts for both x and y directions are reported in Table 25 and Table 26.

Table 25. Peak inter-storey displacement NLTHA results for a PGA of 0.33g.

GM	Peak Displacement X Direction - mm			Peak Displacement Y Direction - mm		
ID	Floor 1	Floor 2	Floor 3	Floor 1	Floor 2	Floor 3
1	15.32	3.09	1.65	1.12	1.04	0.87
2	44.47	5.65	2.47	2.19	2.28	2.17
3	66.09	6.00	2.15	1.68	2.24	2.43
4	24.67	2.44	1.38	1.16	0.97	0.81
5	32.08	4.15	1.48	1.54	1.31	1.16
6	39.13	4.54	1.90	1.16	1.04	1.00
7	25.68	5.97	2.45	1.54	1.33	1.13
8	45.19	6.84	2.78	1.85	1.61	1.64
9	31.11	4.63	1.63	1.40	1.15	0.92
10	35.44	4.85	2.51	1.18	1.27	1.13
11	31.15	5.97	1.91	2.10	1.60	1.42
Mean	**35.48**	**4.92**	**2.03**	**1.54**	**1.44**	**1.33**

Table 26. Peak inter-storey drift NLTHA results for a PGA of 0.33g.

GM	Peak Drift X Direction - %			Peak Drift Y Direction - %		
ID	Floor 1	Floor 2	Floor 3	Floor 1	Floor 2	Floor 3
1	0.57	0.12	0.06	0.04	0.04	0.03
2	1.65	0.23	0.09	0.08	0.09	0.08
3	2.46	0.24	0.08	0.06	0.09	0.09
4	0.92	0.10	0.05	0.04	0.04	0.03
5	1.19	0.17	0.05	0.06	0.05	0.04
6	1.45	0.18	0.07	0.04	0.04	0.04

7	0.95	0.24	0.09	0.06	0.05	0.04
8	1.68	0.27	0.10	0.07	0.06	0.06
9	1.16	0.19	0.06	0.05	0.05	0.03
10	1.32	0.19	0.09	0.04	0.05	0.04
11	1.16	0.24	0.07	0.08	0.06	0.05
Mean	**1.32**	**0.20**	**0.07**	**0.06**	**0.06**	**0.05**

4.2.3 Effective Height Drifts

The maximum drifts evaluated at the effective height of the building are listed in Table 27.

Table 27. Peak effective height drift for NLTHA analyses with a PGA of 0.33g.

GM ID	Peak Effective Height Drift X [%]	Peak Effective Height Drift Y [%]
1	0.28	0.03
2	0.77	0.07
3	1.14	0.06
4	0.43	0.03
5	0.57	0.04
6	0.69	0.03
7	0.49	0.05
8	0.79	0.05
9	0.55	0.04
10	0.64	0.04
11	0.59	0.06
Mean	**0.63**	**0.05**

4.2.4 Base Shear

Table 28. Base shear NLTHA results for a PGA of 0.33g.

GM ID	Governing Failure	Base Shear X [kN]	Base Shear Y [kN]
1	Flexure	+514.89 / -458.51	+949.19 / -769.62
2	Flexure	+760.88 / -707.40	+971.96 / -1185.89
3	Flexure	+611.35 / -716.96	+916.92 / -1025.20
4	Flexure	+391.77 / -616.48	+816.09 / -817.98
5	Flexure	+665.24 / -561.04	+1340.12 / -1120.81
6	Flexure	+609.20 / -627.58	+1093.63 / -935.21
7	Flexure	+740.67 / -464.02	+1018.08 / -1078.61
8	Flexure	+826.39 / -715.22	+1076.79 / -1041.25
9	Flexure	+616.86 / -725.65	+923.51 / -820.92
10	Flexure	+626.67 / -687.15	+916.27 / -845.52
11	Flexure	+738.68 / -648.33	+1325.85 / -831.56
Mean		**+ 645.69 / -629.85**	**+1031.67 / -952.05**

4.2.5 Pier Shear Forces

Force contribution and drift of piers at the peak force for the two directions are listed in Table 29 and Table 30.

Table 29. Pier force and drift at the peak of GM ID 5 site-response hazard in x direction.

Pier	Effective Height [mm]	Displacement at peak [mm]	Drift at peak	Force X at Peak [kN]	Force contribution at Peak
BP11	2690	24.78	0.92%	-0.61	-0.22%
BP12	1890	24.81	1.31%	-2.46	-0.89%
BP13	1890	24.78	1.31%	14.52	5.27%
BP21	2490	4.43	0.18%	-1.28	-0.46%
BP22	2490	4.55	0.18%	-19.34	-7.02%
BP23	2100	3.54	0.17%	9.89	3.59%
FP11	2690	24.43	0.91%	4.98	1.81%
FP12	2690	24.40	0.91%	5.52	2.00%
FP13	1890	24.29	1.29%	12.85	4.66%
FP21	2150	2.36	0.11%	-16.41	-5.96%
FP22	2490	5.24	0.21%	10.07	3.66%
FP23	2490	5.17	0.21%	3.69	1.34%
IP11	2690	24.44	0.91%	4.94	1.79%
IP12	2690	24.68	0.92%	5.81	2.11%
IP13	2690	24.45	0.91%	11.21	4.07%
IP14	2690	24.14	0.90%	3.37	1.22%
IP15	2690	24.14	0.90%	3.37	1.22%
IP16	2690	24.14	0.90%	9.90	3.60%
IP17	2690	23.20	0.86%	5.32	1.93%
IP18	2690	24.07	0.89%	2.37	0.86%
IP21	2490	5.01	0.20%	-5.88	-2.14%
IP22	2490	4.54	0.18%	0.86	0.31%
IP23	2490	4.78	0.19%	8.45	3.07%
IP24	2490	4.63	0.19%	2.03	0.74%
IP25	2490	2.61	0.10%	2.14	0.78%
LG31	2750	1.49	0.05%	-0.75	-0.27%
LP11	2690	24.24	0.90%	-22.09	-8.02%
LP21	2490	5.07	0.20%	-10.95	-3.97%
RG31	2750	1.52	0.06%	3.86	1.40%
RP11	2690	24.73	0.92%	16.88	6.13%
RP21	2490	5.21	0.21%	27.81	10.10%

Table 30. Pier force and drift at the peak of GM ID 5 site-response hazard in y direction.

Pier	Effective Height [mm]	Displacement at peak [mm]	Drift at peak	Force Y at Peak [kN]	Force contribution at Peak
BP11	2690	1.70	0.06%	0.97	0.27%
BP12	1890	1.55	0.08%	0.40	0.11%
BP13	1890	1.31	0.07%	2.20	0.61%
BP21	2490	0.99	0.04%	1.29	0.36%
BP22	2490	1.72	0.07%	1.64	0.46%
BP23	2100	1.74	0.08%	3.95	1.10%

FP11	2690	1.70	0.06%	-0.11	-0.03%
FP12	2690	1.47	0.05%	0.08	0.02%
FP13	1890	1.08	0.06%	-0.88	-0.25%
FP21	2150	1.02	0.05%	-0.15	-0.04%
FP22	2490	1.13	0.05%	-0.28	-0.08%
FP23	2490	1.21	0.05%	0.42	0.12%
IP11	2690	1.51	0.06%	11.53	3.21%
IP12	2690	1.56	0.06%	23.45	6.53%
IP13	2690	2.85	0.11%	-0.77	-0.21%
IP14	2690	3.79	0.14%	-1.35	-0.38%
IP15	2690	3.79	0.14%	-1.35	-0.38%
IP16	2690	2.75	0.10%	1.35	0.38%
IP17	2690	2.03	0.08%	0.06	0.02%
IP18	2690	1.66	0.06%	0.21	0.06%
IP21	2490	1.16	0.05%	9.17	2.55%
IP22	2490	1.19	0.05%	14.71	4.10%
IP23	2490	1.31	0.05%	0.30	0.08%
IP24	2490	1.61	0.06%	0.32	0.09%
IP25	2490	2.51	0.10%	1.62	0.45%
LG31	2750	0.97	0.04%	7.71	2.15%
LP11	2690	1.74	0.06%	18.32	5.10%
LP21	2490	0.98	0.04%	15.62	4.35%
RG31	2750	1.31	0.05%	9.53	2.66%
RP11	2690	1.19	0.04%	13.40	3.73%
RP21	2490	1.47	0.06%	13.53	3.77%

4.2.6 Capacity Curves

The force-displacement curve of each ground motion are depicted in Figure 35. The displacement is recorded at the effective height location.

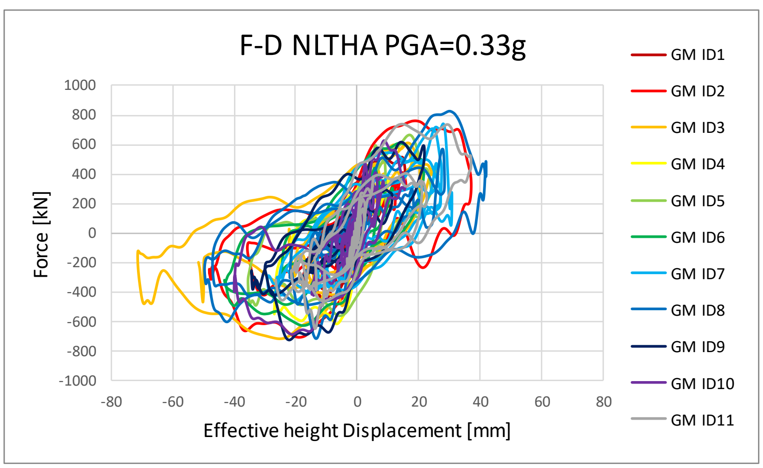

Figure 35. Capacity curves of each ground motion with PGA of 0.33g.

4.3 Comparison NLTHA-NLPO

A backbone curve is derived from the set of performed non-linear time history analyses in order to define an average global behaviour when the building is subjected to an dynamic ground motion. A maximum and a minimum force is extrapolated from each analysis and correlated with the corresponding maximum displacement. An average is made between for the data points from the site-specific hazard analyses. The same procedure is followed for the data points taken from the iterated NLTH analyses. A trilinear backbone curve is obtained and compared with the pushover capacity curves. The maximum positive force of the backbone curve is equal to 613.0 kN while the negative is equal to 598.6 kN at a displacement of 22.21 mm and 31.66 mm, respectively. The collapse displacement is computed by averaging the maximum displacement of the analyses which show a global drift higher than 1.5%. The calculated collapse displacements are 35.0 mm for the positive direction and 56.4 mm for the negative direction, respectively.

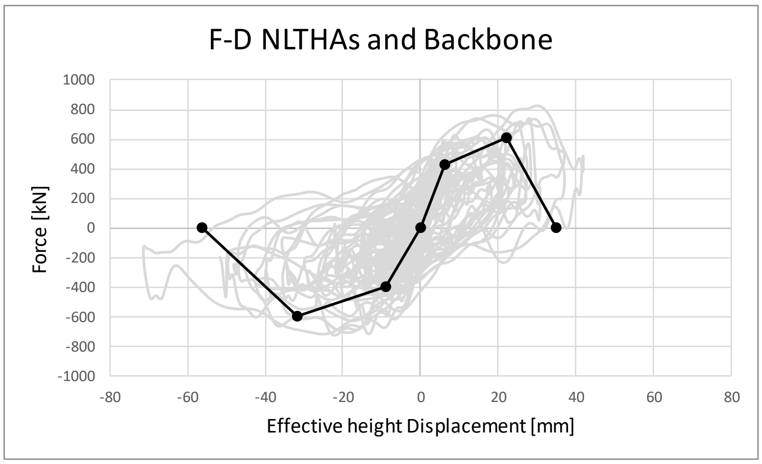

Figure 36. Backbone curve calculated from site-specific and iterated NLTHA analyses.

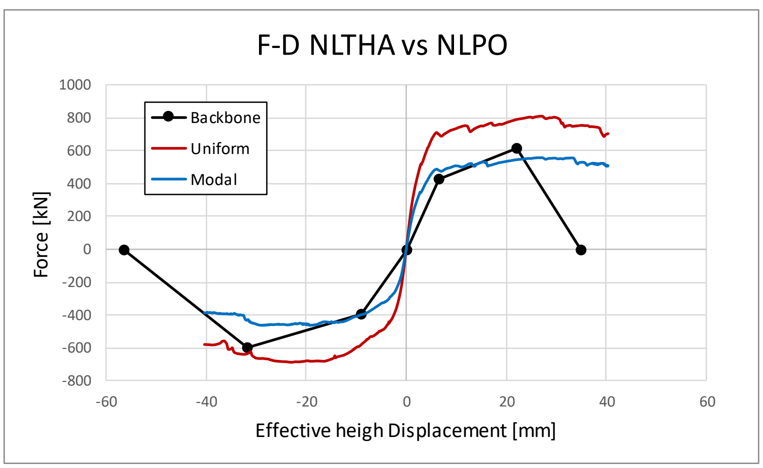

Figure 37. Backbone curve calculated from NLTHA analyses and comparison with NLPO curves.

5 SLaMA ANALYSES

5.1 NPR Assessment For SLaMA Calculations

SLaMA calculations are made according to the following assumptions:

- Discretization in piers and spandrels follows G.9.2.1, based on the identification of the compressive struts in the walls (e.g. below)
- Only inner leaf modelled for resisting system
- Spandrels not analyzed due to presence of RC floors.
- The roof is not modelled, but weight/masses are included
- Vertical load based on initial static configuration & possible flanges
- Two-way spanning RC floors:
    - Able to redistribute the weight of whole structure above
    - Load distributed based on tributary area
    - Double-clamped BC for walls
    - No load transferred to non-loadbearing walls
- Flanges computed according to Moon et al (2006), also for piers connected to inner loadbearing walls
- Contribution non-loadbearing walls computed (but limited)
- Force-displacement behaviour of each pier computed based on G.9.2
- Second order effects considered
- Capacity of each single storey computed separately
- Floors able to redistribute loads among all the piers
- Capacity curve for a storey given by sum of each pier contribution
- Sequence of failure of piers analysed to identify possible local collapse
- Both modal and mass proportional distribution of the lateral loads
- Masses localised at floor level. M0 excluded
- For modal distribution of lateral loads, approximated linear distribution is assumed for sake of simplicity.
- Capacity of each storey normalized based on the effective mass above the floor (M2 for storey level 2, M1+M2 for storey level 1)
- Governing storey level with smallest normalized base shear capacity
- Assessment of governing failure mode
- Analysis of localization of collapse (soft storey?)

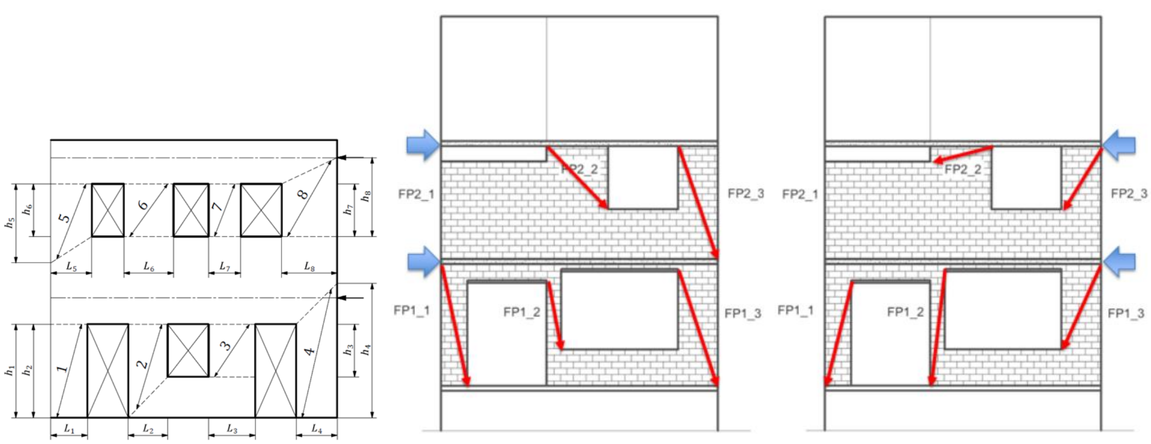

Figure 38. Effective pier height overview for positive loading direction.

Failure type for the positive loading direction is shown in Figure 39. All internal (non-loadbearing) walls fail for flexure (cantilever BC, small vertical load). Ground storey capacity shows (much) smaller respect to the

first storey. Soft storey mechanism is found for both mass- and modal-proportional NLPO. The mechanism is characterized by large ductility (flexure failure governing). The top storey is less ductile, but the mechanism is not activated. The equivalent bilinear capacity curves for positive loading direction are depicted in Figure 41. The mode proportional has a normalized force of 0.084 g and an ultimate displacement of 33.6 mm. The bilinear curves for the negative direction are shown in Figure 42. Respect to the positive direction, the curves exhibit slightly higher acceleration but smaller displacement capacity.
As can be seen in Figure 43, the global failure (connected to the 50% drop of the capacity) occurs earlier than the collapse of all elements of a façade. In the figure, the green pier are failing before the 50% drop, while the red ones, after it. Internal walls provide very small contribution in terms of force, but they results in a very ductile behaviour, mainly due to the small overburden.
The negative mode proportional NLPO is assessed respect to site specific ADRS and to a scaled PGA. The assessment is shown in Figure 44 and Figure 45. The building complaint to NPR9998 for the global in-plane capacity. The scaled PGA which satisfy the displacement demand is equal to 0.171 g.
The SLaMA method is also compared to the FEM calculations in Figure 46. As can be seen, the difference in acceleration is relatively large. NLFEA calculations are between 2.2 and 3.1 times larger than the SLaMA ones. The analytical solution results slightly conservative regarding the near collapse displacement, about 1.2-1.5 times.

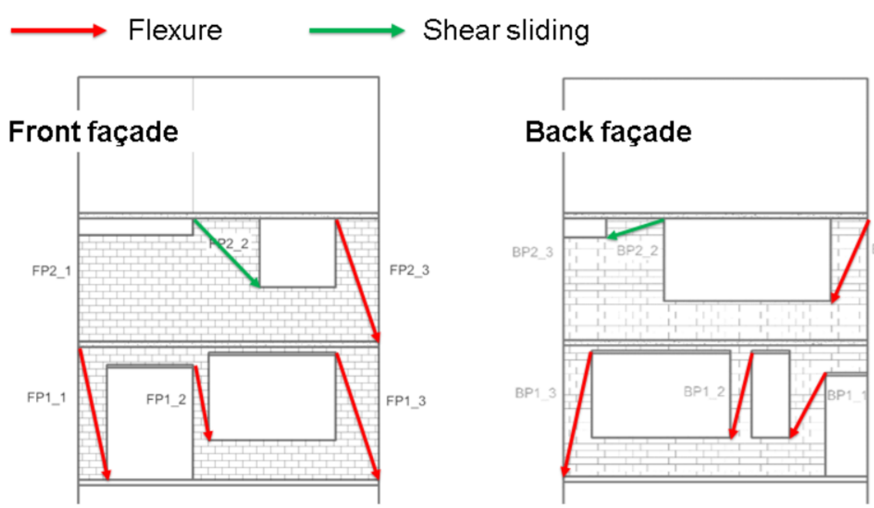

Figure 39. Element failure type of front and back façade for positive loading direction.

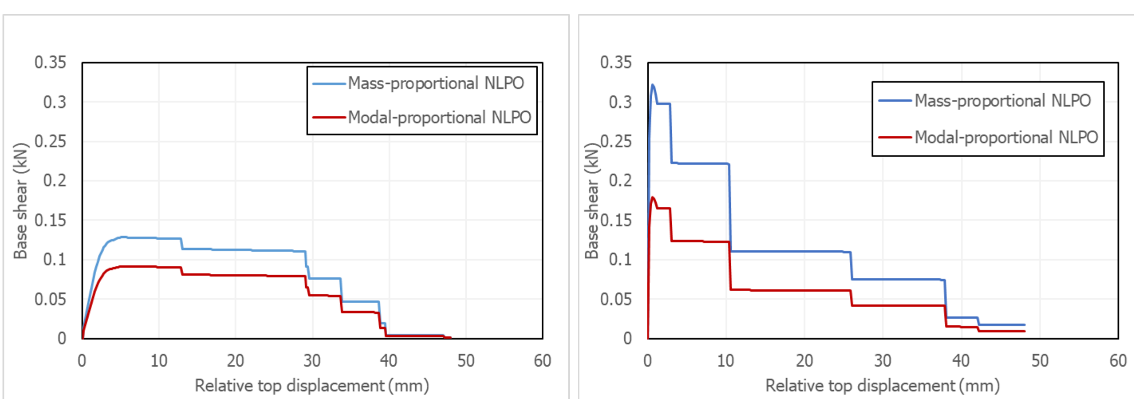

Figure 40. Capacity curve for ground (left) and first (right) storey.

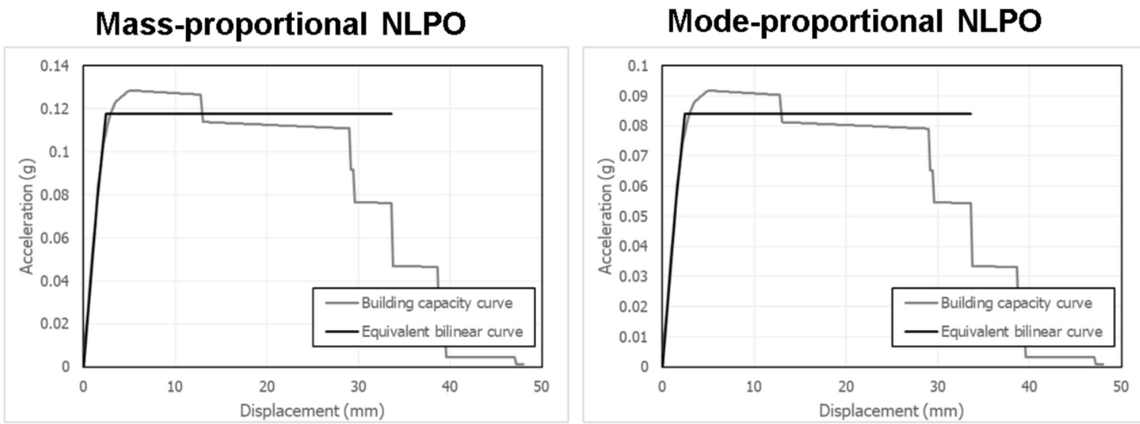

Figure 41. Equivalent bilinear capacity curve for mass and mode proportional, positive loading direction.

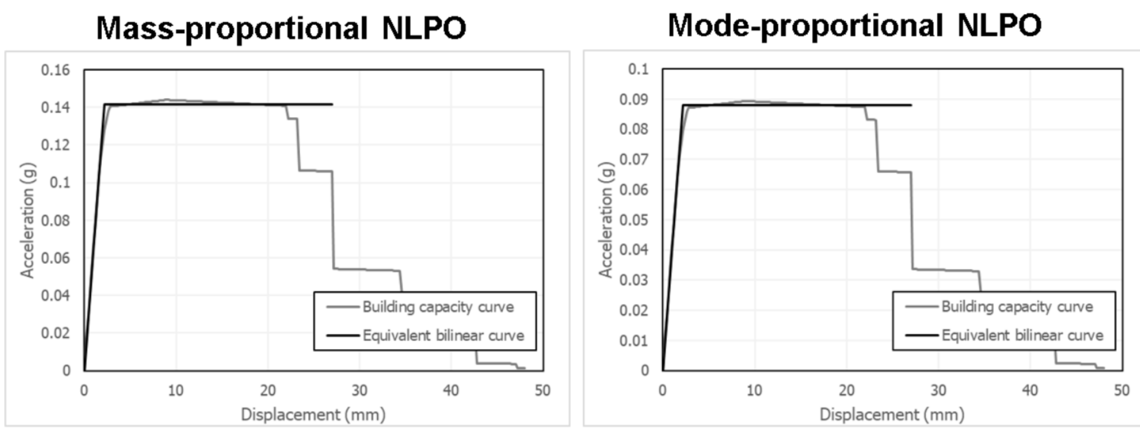

Figure 42. Equivalent bilinear capacity curve for mass and mode proportional, negative loading direction.

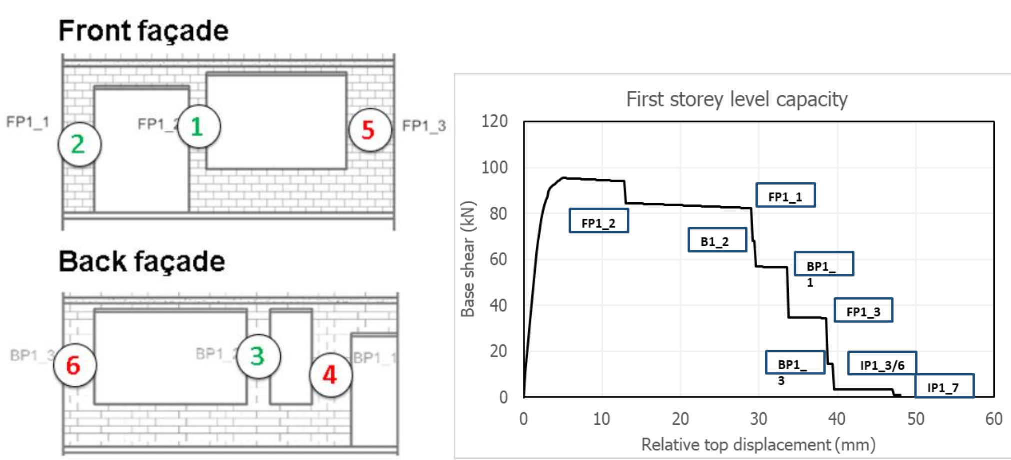

Figure 43. Sequence of NC collapse of the piers.

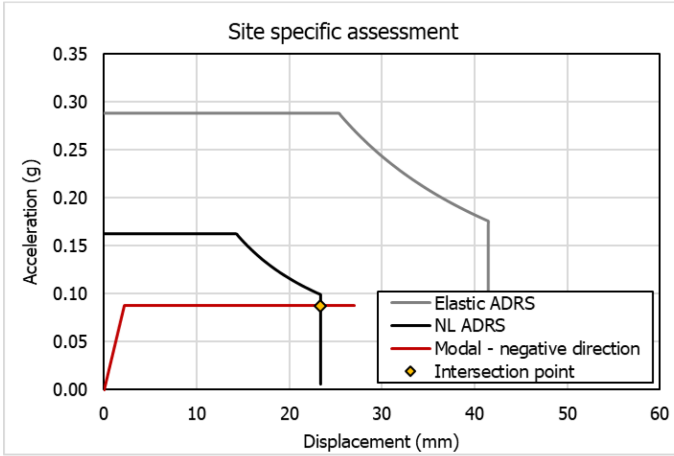

Figure 44. Site specific assessment for mode-proportional NLPO negative loading direction.

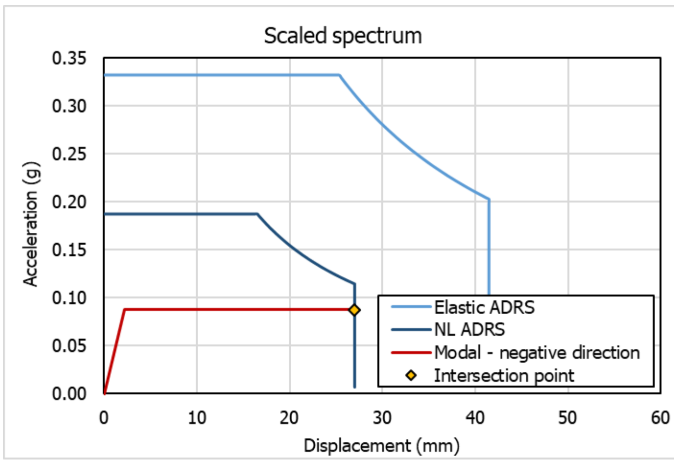

Figure 45. Scaled PGA assessment for mode-proportional NLPO negative loading direction.

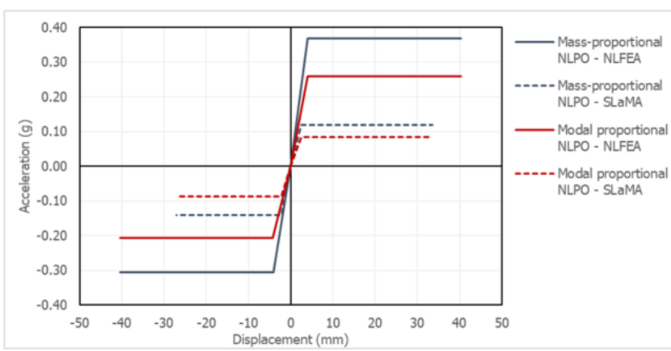

Ratio base shear NLFEA/SLaMA				Ratio NC displacement NLFEA/SLaMA			
Mass-proportional		Modal proportional		Mass-proportional		Modal proportional	
+	-	+	-	+	-	+	-
3.1	2.2	3.1	2.4	1.2	1.5	1.2	1.5

Figure 46. Comparison NLFEA/SLaMA.

Reference

[1] Schreppers et al. 2017 - DIANA FEA report 2016-DIANA-R1601 TU Delft Structural Mechanics CiTG report CM-2016-17, DIANA Validation report for Masonry modelling. 2016 DIANA FEA B.V.

[2] NEN (2018) - Assessment of the structural safety of buildings in case of erection, reconstruction, and disapproval - Induced earthquakes – Basis of design, actions and resistances. NPR9998:2018, NEN.

[3] NEN (2018) - Webtool NPR 9998: Bepaling van de seismische belasting. Available from URL: http://seismischekrachten.nen.nl/

[4] CVW (2018). "Applicatiedocument Beoordeling Seismische Capaciteit (ABSC)". CVW report no. CVW-ABSC-NPR2018-UK.

[5] Arup (2020) - NPR9998_Plan of Approach_Module 4 Phase 3_Rev.0.04, Arup (March, 2020).

Appendix A – Diana Modelling Approach

The modelling approach followed in the software Diana FEA 10.3 is described in the following tables.

Table 31. General modelling description

Input	Description
Analysis Software and Formulation	Diana FEA 10.3 – Implicit Solver
Overview of modelling approach	3D model – non-linear modelling; quadratic curved shell elements, class III beam elements, point interface used as elements. Non-linear pushover and non-linear transient dynamic analysis. Quadrilateral mesh 200x200 mm
Loads	Gravity, equivalent acceleration, modal pushover and base acceleration
Damping	2% Rayleigh Damping

Table 32. Masonry model overview

Input	Description
Element Formulation	Quadratic curved shell elements (CQ40S, CT30S). Full integration scheme 3x3 in the plane and 3 integration points in the thickness of longitudinal façades and 7 integration points in the thickness of transversal façades. Extra dynamic mass to account for veneer, chimney
Material Type	Engineering Masonry Model accounting for cracking, shearing and crushing behaviour. Failure located in integrations point in 4 different directions, horizontal, vertical and two diagonal

Table 33. Timber roof model overview

Input	Description
Element Formulation	Quadratic curved shell elements (CQ40S). Full integration scheme 3x3 in the plane and 3 integration points in the thickness
Material Type	Linear elastic orthotropic material

Table 34. Timber model overview

Input	Description
Element Formulation	Class III beam elements (CL18B). Three integration points in the length
Material Type	Linear elastic isotropic material

Table 35. Interface model overview

Input	Description
Element Formulation	Point interface elements (N6IF)
Material Type	Coulomb friction material

Table 36. Concrete model overview

Input	Description
Element Formulation	Quadratic curved shell elements (CQ40S). Full integration scheme 3x3 in the plane and 3 integration points in the thickness
Material Type	Total Strain Rotating Crack Model

Table 37. Concrete model overview

Input	Description
Element Formulation	Quadratic curved shell elements (CQ40S). Full integration scheme 3x3 in the plane and 3 integration points in the thickness
Material Type	Total Strain Rotating Crack Model

Table 38. Reinforcement model overview

Input	Description
Element Formulation	Distributed grid reinforcement which automatically accounts for bar diameter in the two directions, spacing and concrete cover. Bar reinforcements modelled explicitly for webs of ground floor
Material Type	Von Mises plasticity

Appendix B – Detailed Analysis Results for GM ID 5 Site-Specific Hazard

Table 39. Results overview of GM ID 5 site-specific hazard.

GM ID 5 - Data	Value
Peak Displacement X Direction Floor 1 - mm	8.99
Peak Displacement X Direction Floor 2 - mm	1.08
Peak Displacement X Direction Floor 3 - mm	0.72
Peak Displacement Y Direction Floor 1 - mm	0.44
Peak Displacement Y Direction Floor 2 - mm	0.38
Peak Displacement Y Direction Floor 3 - mm	0.27
Peak Drift X Direction Floor 1 - %	0.33
Peak Drift X Direction Floor 2 - %	0.04
Peak Drift X Direction Floor 3 - %	0.03
Peak Drift Y Direction Floor 1 - %	0.02
Peak Drift Y Direction Floor 2 - %	0.02
Peak Drift Y Direction Floor 3 - %	0.01
Peak Effective Height Drift X [%]	0.16
Peak Effective Height Drift Y [%]	0.01
Base Shear X [kN]	+430.10 / -362.28
Base Shear Y [kN]	+472.64 / -428.93

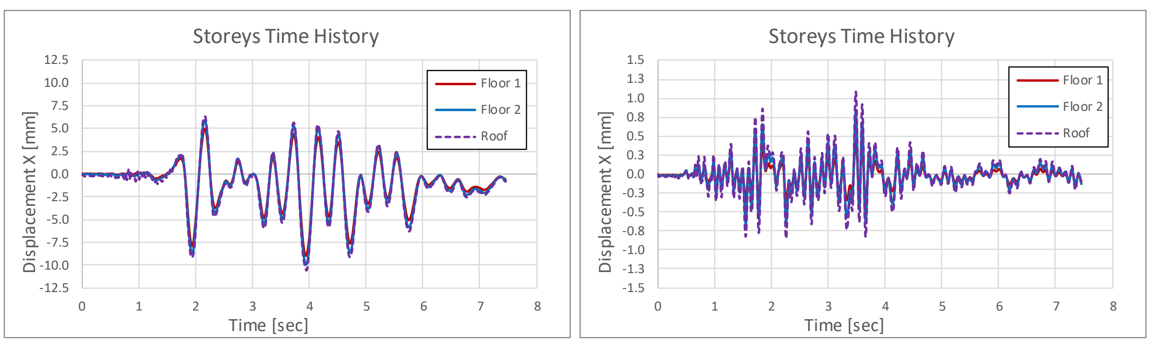

Figure 47. Inter-storey drift time histories in direction X and Y.

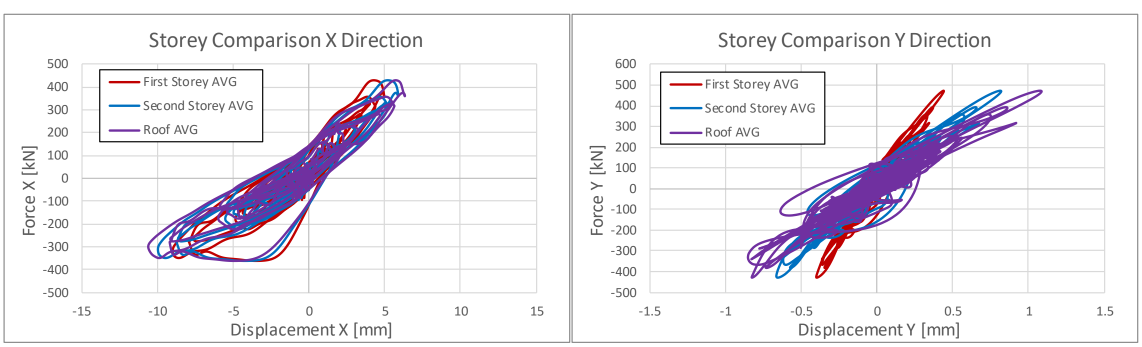

Figure 48. Force-Displacement of different storeys in direction X and Y.

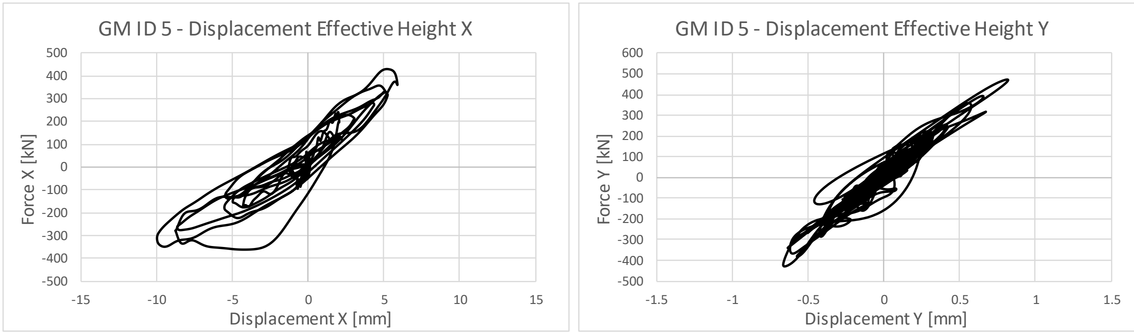

Figure 49. Force-Displacement at effective height in direction X and Y.

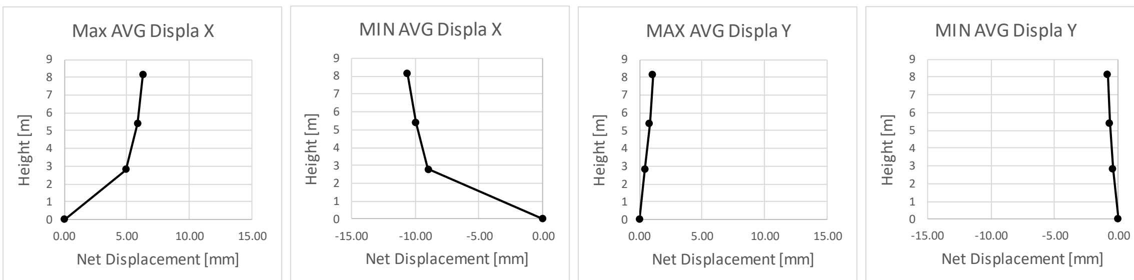

Figure 50. Deformed shape in direction X and Y.

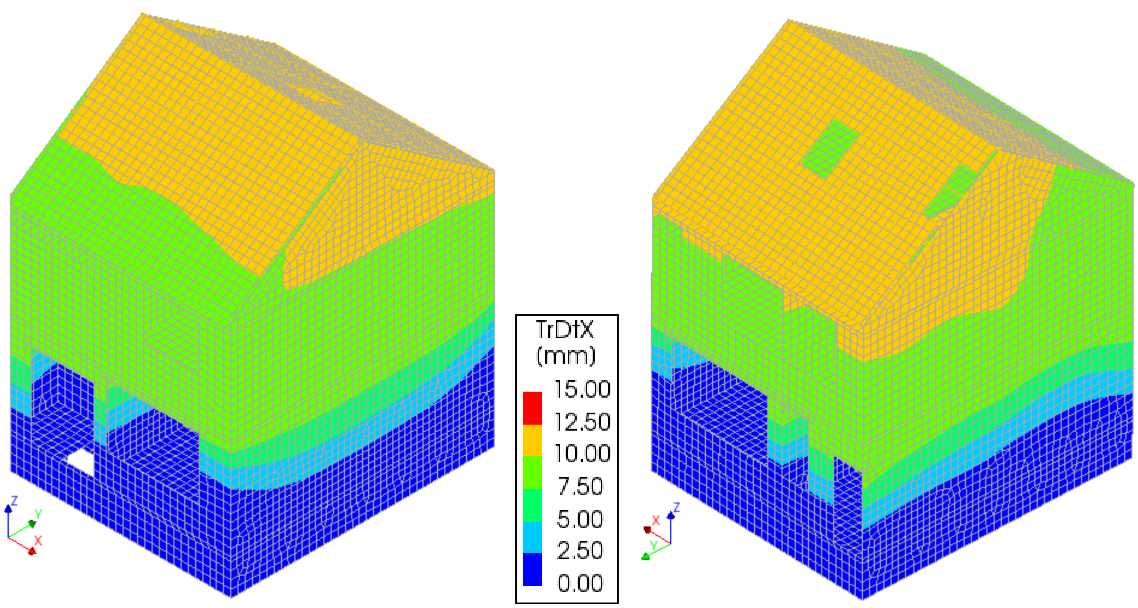

Figure 51. External walls absolute maximum displacement in X direction. Front and back view.

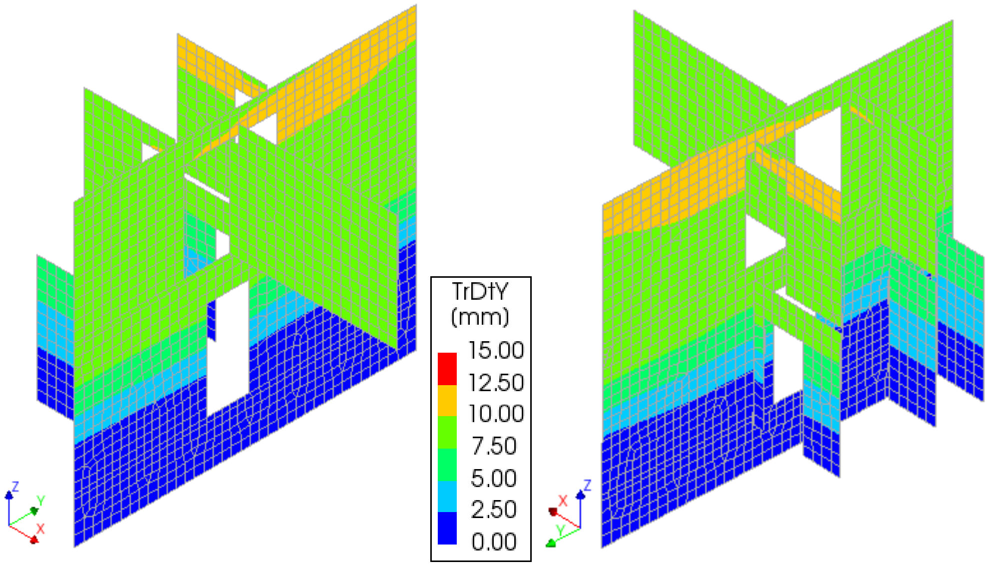

Figure 52. Internal walls absolute maximum displacement in X direction. Front and back view.

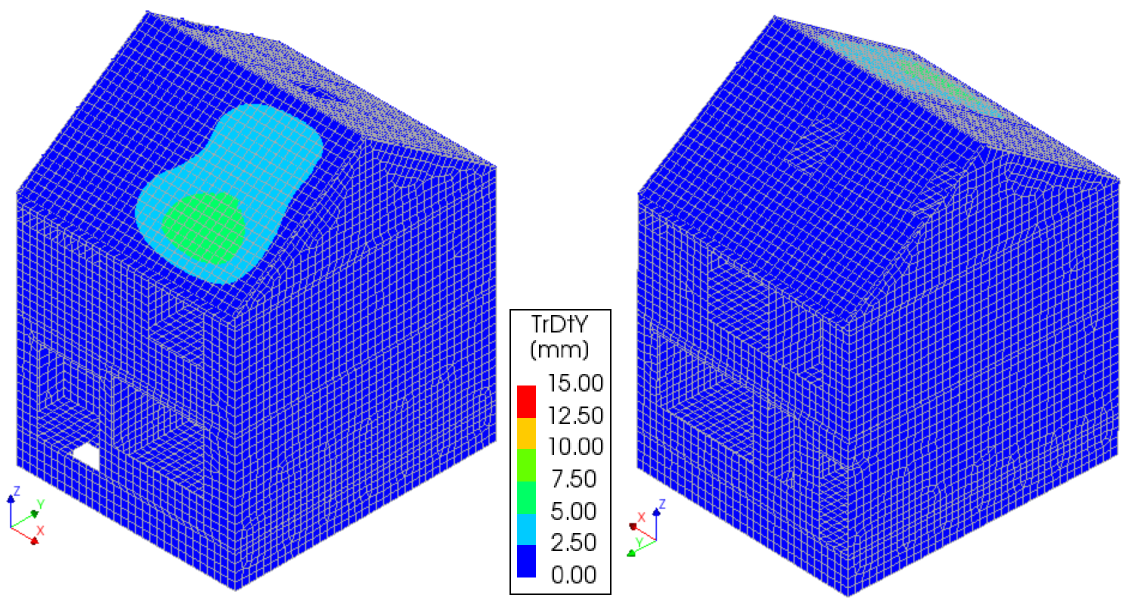

Figure 53. External walls absolute maximum displacement in Y direction. Front and back view.

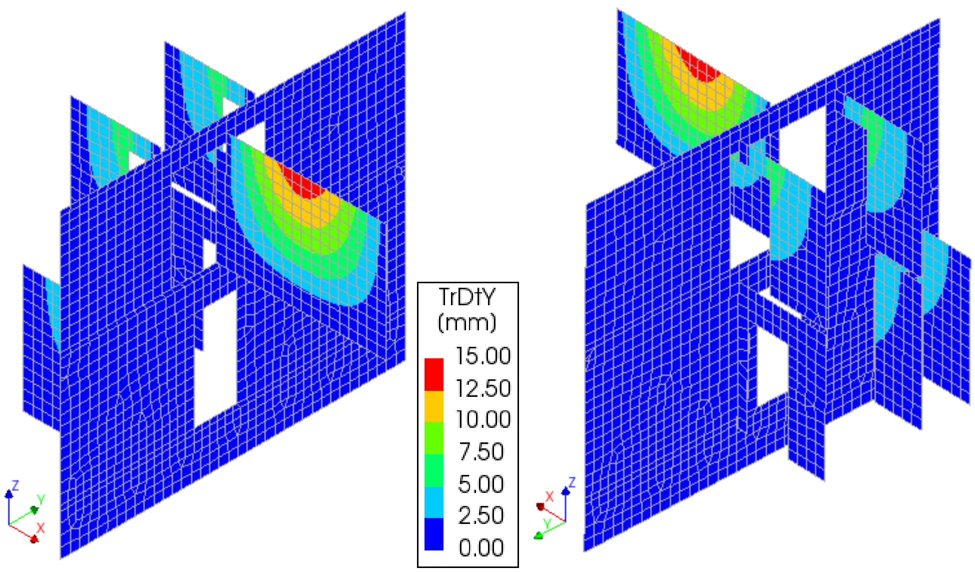

Figure 54. Internal walls absolute maximum displacement in Y direction. Front and back view.

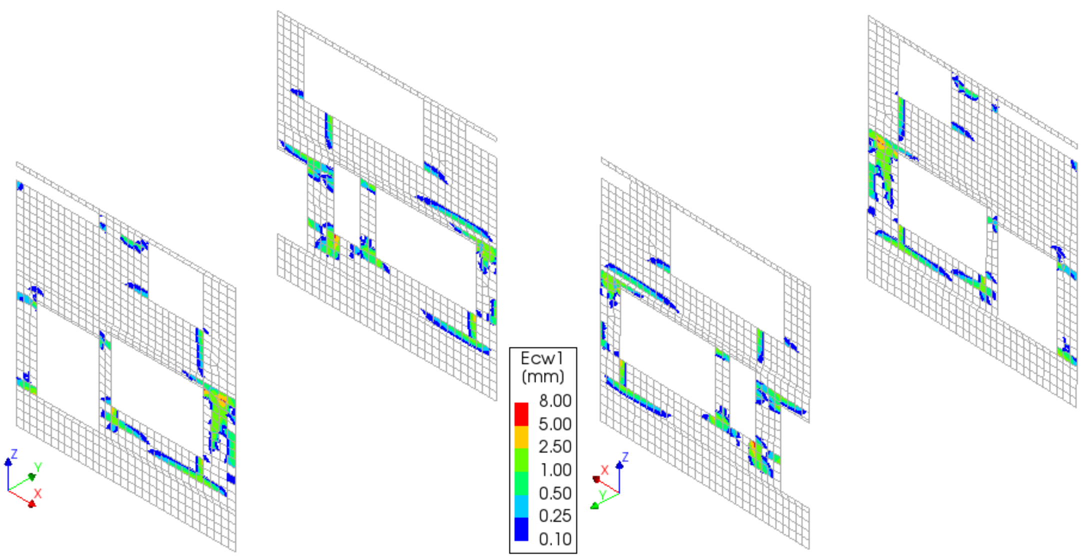

Figure 55. Max recorded principal crack width of external longitudinal walls. Front and back view.

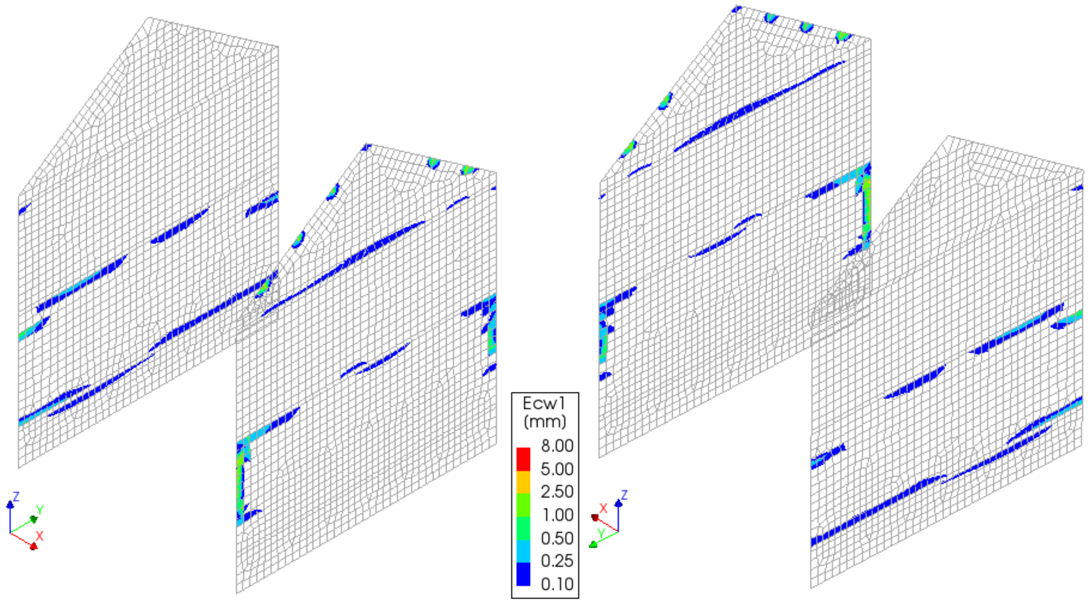

Figure 56. Max recorded principal crack width of external transversal walls. Front and back view.

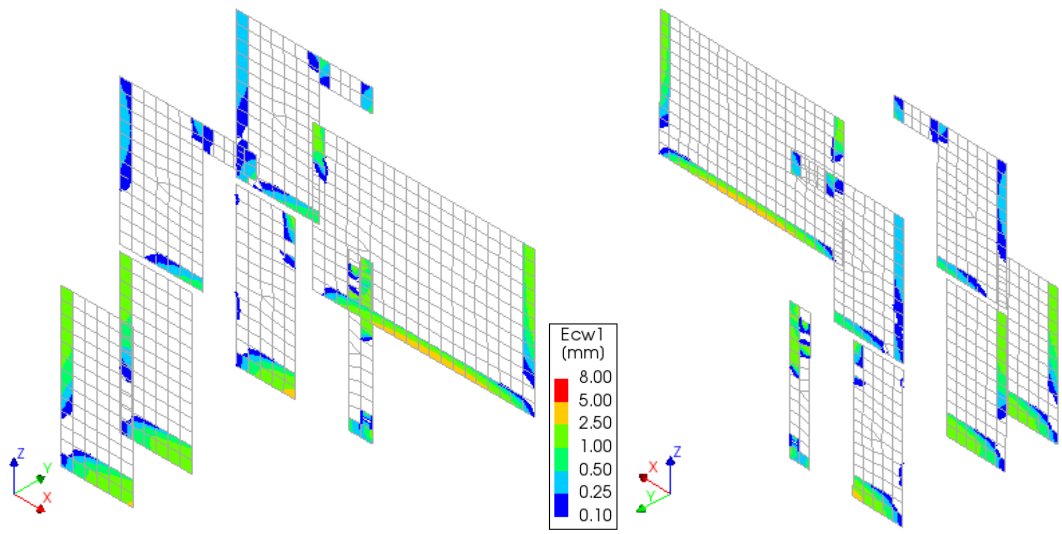

Figure 57. Max recorded principal crack width of internal longitudinal walls. Front and back view.

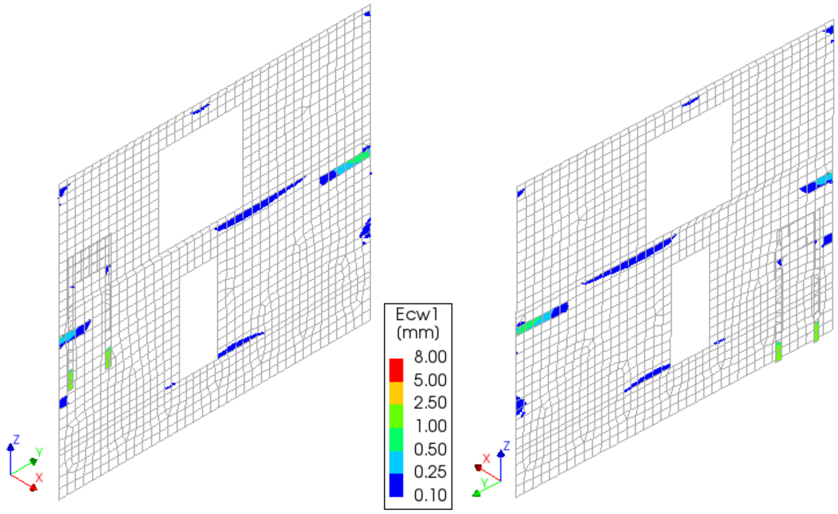

Figure 58. Max recorded principal crack width of internal transversal walls. Front and back view.

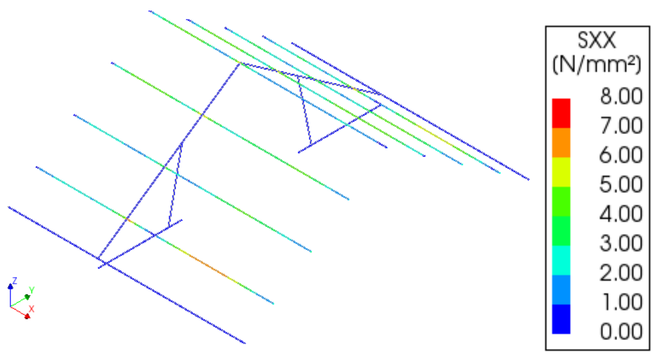

Figure 59. Peak of global X stress of roof beams.

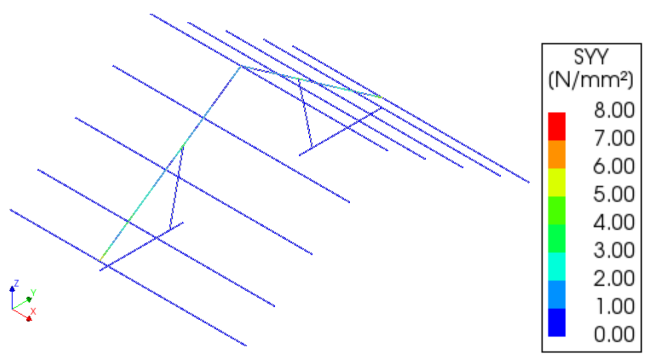

Figure 60. Peak of global Y stress of roof beams.

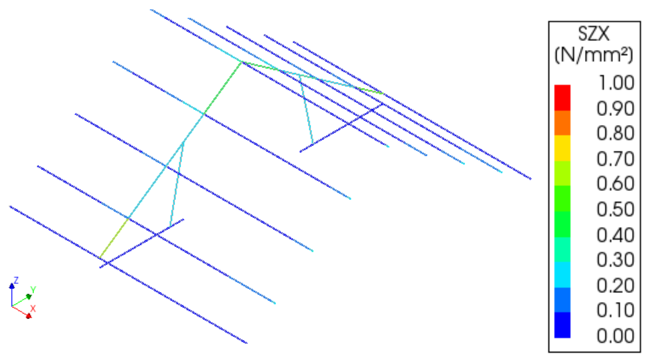

Figure 61. Peak of global ZX shear stress of roof beams.

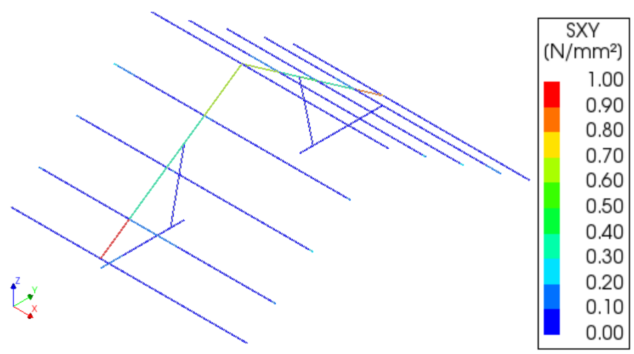

Figure 62. Peak shear stress XY of roof diaphragm.

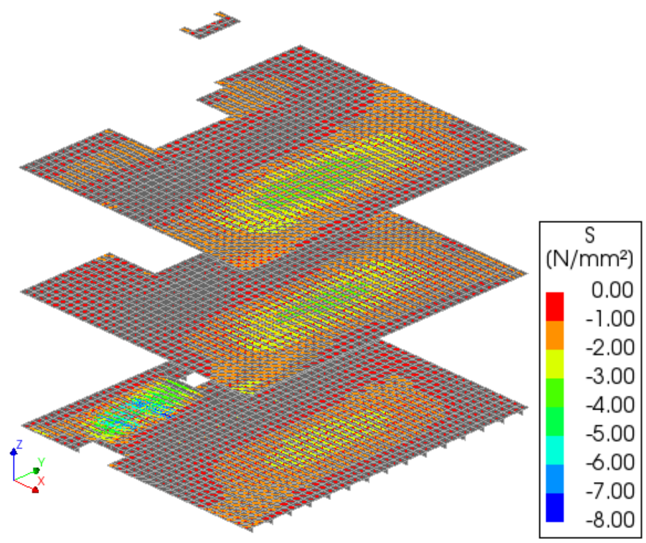

Figure 63. Peak principal compressive stress at top of concrete floors – Layer 7.

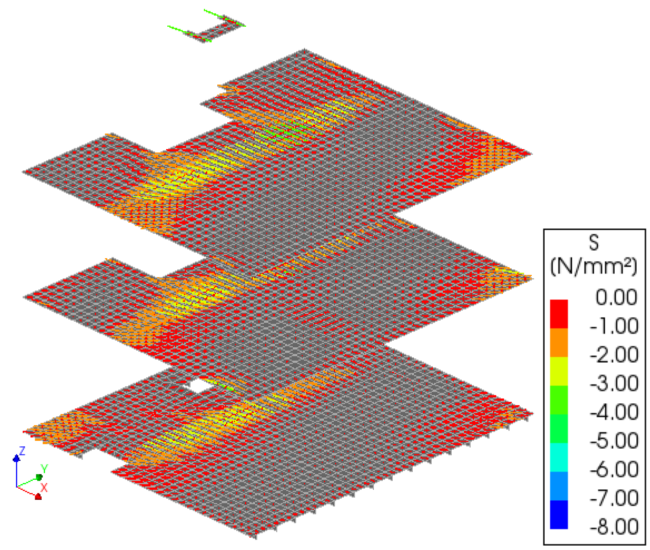

Figure 64. Peak principal compressive stress at bottom of concrete floors – Layer 1.

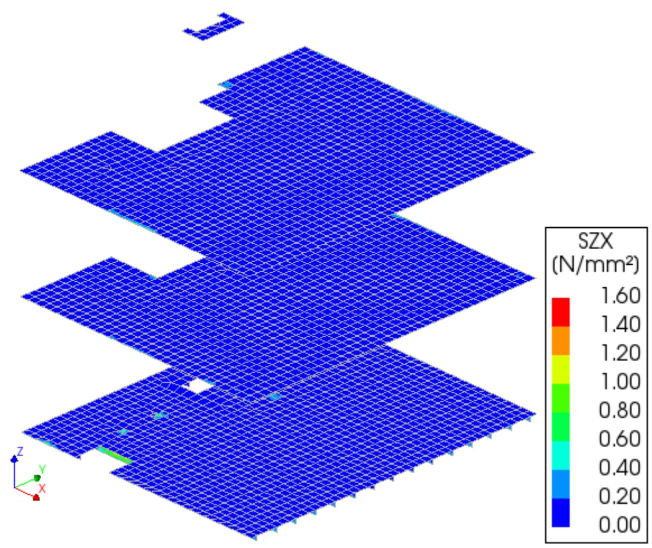

Figure 65. Peak shear stress XZ of concrete floors.

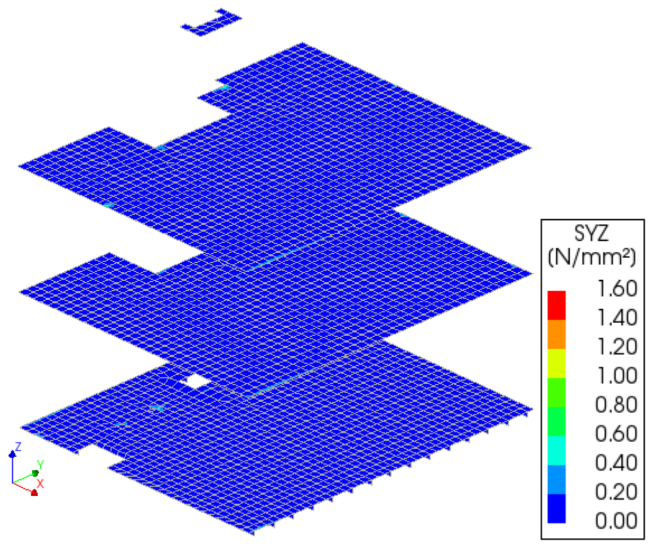

Figure 66. Peak shear stress YZ of concrete floors.